Hydraulic Effects of Drill-String Tool Joint and Rotation on Annular Flow Profile and Frictional Pressure Loss Using ANSYS-CFX

by

Lek Chun Hou

14876

Dissertation submitted in partial fulfilment of

the requirements for the

Degree of Engineering (Hons)

Petroleum

January 2015

Universiti Teknologi PETRONAS
Bandar Seri Iskandar
32610 Tronoh
Perak Darul Ridzuan

CERTIFICATION OF APPROVAL

Hydraulic Effects of Drill-String Tool Joint and Rotation on Annular Flow Profile and Frictional Pressure Loss Using ANSYS-CFX

by

Lek Chun Hou
14876

A project dissertation submitted to the
Petroleum Engineering Programme
Universiti Teknologi PETRONAS
in partial fulfilment of the requirement for the
BACHELOR OF ENGINEERING (Hons)
PETROLEUM

Approved by,

_____

Titus Ntow Ofei

UNIVERSITI TEKNOLOGI PETRONAS
TRONOH, PERAK
January 2015

CERTIFICATION OF ORIGINALITY

This is to certify that I am responsible for the work submitted in this project, that the original work is my own except as specified in the references and acknowledgements, and that the original work contained herein have not been undertaken or done by unspecified sources or persons.

_____

LEK CHUN HOU

ABSTRACT

In oil and gas well drilling, inaccurate estimation of drilling parameters can affect the predictions of annular flow profile and frictional pressure loss along the wellbore which can result in hole problems, such as hole erosion due to high annular fluid velocity, and inadequate drill cuttings transport, well control issues such as kick or lost circulation. Drill-string tool joints alter the annular geometry, when coupled with drill-string rotation, they affect the annular flow profile and frictional pressure loss by causing turbulence, fluid acceleration/deceleration or changing the drilling mud apparent viscosity. As the oil and gas industry moves towards deeper wells, drilling operation uses more drill-string tool joints, the additional frictional pressure loss can be significant, up to 30% of the total frictional pressure loss. Therefore, there is a need to better understand the effects of drill-string tool joint and pipe rotation on annular flow profile and frictional pressure loss. The objective of this study was to analyse individually and collectively the hydraulic effects of drill-string tool joints and rotation on annular flow profile and frictional pressure loss. The scope and methodology of this research involved Computational Fluid Dynamics (CFD) approach, with ANSYS-CFX (in ANSYS 15) as the analysis system, where a CFD model with an optimum mesh size was created and validated against previous experimental data, where frictional pressure loss values were compared. Excellent agreement was achieved, the Mean Percentage Error ranged from 0.5% to 23.9%. The fluid was modelled using Power Law rheology. A horizontal wellbore with a concentric and rotating drill-string was considered where the fluid flow was assumed laminar, steady state and fully developed. The temperature condition is isothermal. Upon validating the CFD model, case studies based on design points were carried out to evaluate the factors and responses of this project and better understand the relationships between different parameters. The results had shown that the highest fluid velocity was at the tool joint section. As the drill-string rotation speed increased, the velocity of the fluid immediately next to the drill-string outer wall increased by 98.4%. On the other hand, frictional pressure loss increased by 55.9% when a tool joint was present. Frictional pressure loss decreased as much as 18.6% as the drill-string rotation speed increased. In conclusion, this project aimed at understanding the hydraulic effects of drill-string tool joints and rotation on annular flow profile and frictional pressure loss, and hence promote efficient well design and safe drilling operations in the ever-challenging oil and gas industry.

ACKNOWLEDGEMENT

This project was fully supported by Universiti Teknologi PETRONAS. The author wishes to express his utmost gratitude to Mr Titus Ntow Ofei who provided insight and expertise, continuous support and guidance that greatly assisted in the completion of this study.

In addition, Dr Tamiru Alemu Lemma, as the Internal Examiner for this project, also suggested constructive advices which helped to improve the quality of methodology and result analysis for this study. Besides, Dr Syahrir Ridha, as the Final Year Project Coordinator had been very helpful in ensuring the schedule of this project can be achieved in a timely manner.

Last but not least, the author wishes to show his appreciation to all parties involved in this project.

TABLE OF CONTENTS

ABSTRACT 1
ACKNOWLEDGEMENT 2
LIST OF FIGURES 5
LIST OF TABLES 7
ABBREVIATION AND NOMENCLATURE 8
CHAPTER 1 9
1. INTRODUCTION 9
1.1 Background 9
1.2 Problem Statement 10
1.3 Objectives 10
1.4 Scope of Study 10
CHAPTER 2 12
2. LITERATURE REVIEW 12
2.1 Power Law Drilling Mud 12
2.2 Effects of Drill-string Tool Joint 12
2.3 Effects of Drill-String Rotation 13
2.4 Annular Flow Profile 14
2.5 Frictional Pressure Loss 14
CHAPTER 3 15
3. METHODOLOGY 15
3.1 Computational Fluid Dynamics (CFD) Approach 15
3.2 ANSYS-CFX Work Flow 16
3.2.1 Geometry 16
3.2.2 Mesh 19
3.2.3 Setup: Physics And Boundary Conditions Modelling 21
3.2.4 Solution: CFD Model Solving 21
3.2.5 Results: Simulation Result Collection And Analysis 22
3.3 Main Project Stages 23
3.3.1 Grid Independence Study 23
3.3.2 Benchmarking: CFD Model Validation With Experimental Data 24
3.3.3 Design of Experiment: Case Study Based On Design Points 30

3.4 Project Key Milestones....31
3.5 Project Timeline – Gantt Chart....32
3.6 Simulation Flow Chart....33
CHAPTER 4....34
4. RESULT AND DISCUSSION....34
4.1 Hydraulic Effects of Drill-String Tool Joint on Annular Flow Profile and Frictional Pressure Loss....34
4.2 Hydraulic Effects of Drill-String Rotation on Annular Flow Profile and Frictional Pressure Loss....38
4.3 Combined Effects of Drill-String Tool Joint and Rotation on Annular Flow Profile and Frictional Pressure Loss....44
CHAPTER 5....46
5. CONCLUSION & RECOMMENDATIONS....46
5.1 Conclusion....46
5.2 Recommendations....47
REFERENCES....48
APPENDICES....ii
Appendix 1: ANSYS-CFX Simulation Result Formats....ii
Appendix 2: Benchmarking - CFD Model Adjustments To Improve Benchmarking....iii
Appendix 3: Benchmarking – Tabulated Results....v
Appendix 4: Design of Experiment – Tabulated Results....vii

LIST OF FIGURES

Figure 1: CFD project schematic in ANSYS Workbench under ANSYS-CFX analysis system....16
Figure 2: 3D view of CFD model geometry in DesignModeler....17
Figure 3: Close up view of CFD model geometry: Drill-string tool joint section....17
Figure 4: Physical model....18
Figure 5: Geometry of the CFD model for "Design of Experiment: case study based on design points" stage (not-to-scale sketch)....19
Figure 6: Meshing (longitudinal view)....20
Figure 7: Meshing (cross-sectional view)....20
Figure 8: CFX-Solver Manager simulation monitor....22
Figure 9: Grid independence study (graph)....24
Figure 10: Frictional pressure loss between CFD simulation and experimental results for fluid E at P1: 36" tool joint section....26
Figure 11: Frictional pressure loss between CFD simulation and experimental results for fluid E at P2: 12" section without tool joint....26
Figure 12: Frictional pressure loss between CFD simulation and experimental results for fluid E at P3: 12" tool joint section....27
Figure 13: Frictional pressure loss between CFD simulation and experimental results for fluid G at P2: 12" section without tool joint....28
Figure 14: Frictional pressure loss between CFD simulation and experimental results for fluid G at P3: 12" tool joint section....28
Figure 15: Frictional pressure loss values between CFD simulation and experimental results for fluid G at P2: 12" section without tool joint....29
Figure 16: Frictional pressure loss values between CFD simulation and experimental results for fluid G at P3: 12" tool joint section....29
Figure 17: Gantt Chart....32
Figure 18: Simulation flow chart....33
Figure 19: Annular flow profile without tool joint....34
Figure 20: Annular flow profile with 1 tool joint....34
Figure 21: Annular flow profile with 2 tool joints....35

Figure 22: Frictional pressure loss along the annulus at 0 RPM with no tool joint.....36
Figure 23: Frictional pressure loss along the annulus at 0 RPM with 1 tool joint.....36
Figure 24: Frictional pressure loss along the annulus at 0 RPM with 2 tool joints 36
Figure 25: Pressure loss versus number of tool joint at 0 RPM drill-string rotation speed 37
Figure 26: Annular flow profile at 0 RPM without tool joint.....38
Figure 27: Annular flow profile at 300 RPM without tool joint.....38
Figure 28: Annular flow profile at 600 RPM without tool joint.....39
Figure 29: Velocity profile at the outlet at 0 RPM without tool joint.....40
Figure 30: 2D (left) and 3D (right) velocity profile at the outlet at 0 RPM without tool joint 40
Figure 31: 2D (left) and 3D (right) dynamic viscosity profile at the outlet at 0 RPM without tool joint.....41
Figure 32: Velocity profile at the outlet at 600 RPM without tool joint.....41
Figure 33: 2D (left) and 3D (right) velocity profile at the outlet at 600 RPM without tool joint 42
Figure 34: 2D (left) and 3D (right) dynamic viscosity profile at the outlet at 600 RPM without tool joint.....42
Figure 35: Pressure loss versus drill-string rotation without tool joint.....43
Figure 36: Annular flow profile at 600 RPM with 1 tool joint.....44
Figure 37: Frictional pressure loss versus drill-string rotation for 0 and 1 tool joint 45
Figure A-1.1: Graph of pressure versus the entire annulus length……..……..…i
Figure A-1.2: Velocity streamline……..……..……i
Figure A-1.3: Dynamic viscosity contour……..……....ii
Figure A-1.4: Volume rendering of pressure distribution in CFD-Post……..…..……...ii

LIST OF TABLES

Table 1: General geometry of the CFD model 18

Table 2: Number of mesh element used in grid independence study 23

Table 3: Grid independence study (table) 23

Table 4: Power Law Fluids Properties 25

Table 5: Design of Experiment 30

Table 6: Project Key Milestones 31

Table A-2.1: Adjustments made on CFD model to improve Benchmarking……...……iii

Table A-3.1: P1: 36” tool joint section pressure loss values at various flow rates for fluid E at 0 RPM (CFD simulation and experimental results)……...…….v

Table A-3.2: P2: 12” section without tool joint pressure loss values at various flow rates for fluid E at 0 RPM (CFD simulation and experimental results)……..……v

Table A-3.3: P3: 12” tool joint section pressure loss values at various flow rates for fluid E at 0 RPM (CFD simulation and experimental results)……..…….v

Table A-3.4: P2: 12” section without tool joint pressure loss values at various flow rates for fluid G 60 RPM and 180 RPM (CFD simulation and experimental results)…….…..….v

Table A-3.5: P3: 12” tool joint section pressure loss values at various flow rates for fluid G for 60 RPM and 180 RPM (CFD simulation and experimental results)…….……..vi

Table A-4.1: Frictional pressure loss due to tool joint(s) at 0 RPM drill-string rotation speed…….vii

Table A-4.2: Frictional pressure loss due to drill-string rotation without tool joint…...vii

Table A-4.3: Frictional pressure loss due to drill-string tool joint(s) and rotation…….viii

ABBREVIATION AND NOMENCLATURE

CFD: Computational Fluid Dynamics

ECD: Equivalent Circulating Density

ID: Inner diameter

MPE: Mean Percentage Error

OD: Outer diameter

RPM: Rotation per Minute

USGPM: US Gallon per Minute

CHAPTER 1

1. INTRODUCTION

1.1 Background

In this study, the hydraulic effects of drill-string tool joint and rotation on annular flow profile and frictional pressure loss are studied in ANSYS-CFX (ANSYS-15) by CFD simulation.

For annular flow profile, annular velocity that is too high will promote hole erosion while too low will cause inadequate drill cuttings transport. On the other hand, accurate prediction of frictional pressure loss is important in: designing hydraulics program and well control (controlling ECD) [1] - [2], slim hole well, formation with narrow drilling window between pore pressure and fracture pressure, swab and surge conditions, narrow clearance extended reach well, Managed Pressure Drilling, Underbalanced Drilling [3] - [4] , completion, fracturing, acidizing, workover and production [5].

Vajargah et al. [4] have shown that drill-string tool joints can contribute significantly to frictional pressure loss, especially in deeper wells. Estimating frictional pressure loss with drill-string tool joints is challenging due to the fact that the drilling mud is Non-Newtonian, exhibits time dependent characteristic and temperature variation along the wellbore [1]. In addition, rotation of the drill-string complicates the matter further.

The effect of drill-string rotation is not well understood, many field measurements reported that frictional pressure loss increases with rotation, increasing wellbore pressure and ECD [1]. Researchers [1], [3], [6] – [17] have shown that frictional pressure loss may increases or decrease with rotation, mainly depending on the fluid rheology.

1.2 Problem Statement

Inaccurate estimation of drilling parameters can affect the predictions of annular flow profile and frictional pressure loss along the wellbore which can result in hole problems, such as hole erosion/inadequate drill cuttings transport, kick or lost circulation.

Drill-string tool joints alter the annular geometry, when coupled with drill-string rotation, they affect the annular flow profile and frictional pressure loss by causing turbulence, fluid acceleration/deceleration or changing the drilling mud apparent viscosity.

As the oil and gas industry moves towards deeper wells, drilling operation uses more drill-string tool joints, the additional frictional pressure loss can be significant, up to 30% of the total frictional pressure loss [4]. As for annular flow profile, annulus velocity that is too high will promote hole erosion while too low will cause inadequate drill cuttings transport. Therefore, there is a need to better understand the effects of drill-string tool joint and drill pipe rotation on annular flow profile and frictional pressure loss.

1.3 Objectives

The objectives of this study are outlined below:

- To analyse the hydraulic effects of drill-string tool joints on annular flow profile and frictional pressure loss.
- To analyse the hydraulic effects of drill-string rotation on annular flow profile and frictional pressure loss.
- To predict the combined effect of drill-string rotation and tool joint on annular flow profiles and frictional pressure loss.

1.4 Scope of Study

This study investigates the variations in annular flow profile and frictional pressure loss due to (1) drill-string tool joints and (2) drill-string rotation. The research will be carried out using the Computational Fluid Dynamics (CFD) approach, with ANSYS-CFX as the analysis system, where a CFD model will be created and validated against previous experimental data. The fluid will be modelled using Power Law rheology. A horizontal wellbore with a concentric and rotating drill-string is considered where the fluid flow is

assumed laminar, steady state and fully developed. The temperature condition is isothermal. Upon validating the CFD model, case studies based on design points and further parametric studies will be carried out to evaluate different design scenarios and better understand the relationships between different parameters.

CHAPTER 2

2. LITERATURE REVIEW

There are different researches on evaluating the hydraulic effects of drill-string tool joint and/or drilling string rotation on annular flow profile and/or frictional pressure loss. These researches employ different approaches, i.e. experimental approach [2], [5], [7] - [14], theoretical approach [6], [15], [16], or Computational Fluid Dynamics (CFD) approach [1], [3], [4], [17] - [19], [20].

2.1 Power Law Drilling Mud

Bared [6] explains that the mathematical expression for this rheology is: $\tau = K\gamma^n$ where τ is the shear stress, K is the consistency index which describes the pumpability of the fluid (the higher the value of K, the higher the frictional pressure loss), γ is the shear rate, n is the flow behavior index, n < 1, shear thinning. The rotation of drill-string will affect the value of K and n constants, which means the apparent viscosity of Power Law fluid is subject to change under rotation.

2.2 Effects of Drill-string Tool Joint

Drill-string tool joint outer diameter (OD) is larger than the OD of drill pipe, and inner diameter (ID) is smaller than the ID of drill pipe. These external and internal upsets forms contraction and expansion zones that create flow disturbance to the flow of fluid in the wellbore.

Field data [1] and CFD approach have shown that excessive frictional pressure loss exist through drill-string tool joint. This is because the annular space around the tool joint section is smaller, which leads to a higher fluid velocity and Reynolds number, hence turbulent flow condition tends to be established [2]. Dokhani et al. [18] found that without drill-string rotation, squared tool joint increases frictional pressure loss up to 42% while

tapered tool joint is up to 26%. The higher the angle of convergence and divergence, the higher the frictional pressure loss [5], [19].

2.3 Effects of Drill-String Rotation

According to Bared [6], the frictional pressure loss calculations in the oil field always assume the drill-string and annulus as a static or motionless system. When the drill-string is rotating, the frictional pressure loss is different than in static condition, due to a change in the fluid average velocity and apparent viscosity that affect the Reynolds number and Fanning friction factor. Different researches found contradicting effects of drill-string rotation. According to Chandrasekhar [21], there are two different effects of drill-string rotation on frictional pressure loss; firstly, rotation increases frictional pressure loss for low viscosity fluid due to the onset of centrifugal instabilities. Secondly, rotation decreases frictional pressure loss for high viscosity shear thinning fluid. Similarly, McCann et al. [8] used a specially designed slim hole flow loop and found that rotation increases frictional pressure loss in turbulent flow, while rotation decreases frictional pressure loss in laminar flow. The experiments conducted by Hemphill et al. [13] and Ozbayoglu et al. [14] suggested that drill-string rotation increases frictional pressure loss. There were several studies [9] – [11] where frictional pressure loss has been determined from real field wells. These authors concluded that drill-string rotation increases the frictional pressure loss. On the contrary, Walker and Othmen [12] conducted an experiment and found that frictional pressure loss decreases with increased drill-string rotation. They used a viscous shear thinning fluid and fairly narrow annuli, which the latter suppresses centrifugal instability. Besides, Hansen and Sterri [7] also carried out an experiment with 50% eccentricity, rotation speed of 0, 300 and 600 rpm. The fluid in use was a highly viscous shear thinning fluid where the fluid flow under rotation had no centrifugal instability and was laminar flow. The result was up to 20% decrease in frictional pressure loss. It is worth noting that Taylor number was used to characterise the onset of centrifugal instability; below the critical Taylor number, the flow regime is laminar and centrifugal instability is not present [20]. Under this condition, increasing drill-string rotation speed decreases the frictional pressure loss. In addition, Luo and Peden [16] suggested that drill-string rotation decreases frictional pressure loss.

2.4 Annular Flow Profile

Critical velocity is a term that enables us to distinguish whether the flow regime is laminar or turbulent [6]. If the average velocity of the fluid is greater than the critical velocity, the flow is turbulent, otherwise, the flow is laminar. Typically, the fluid velocity in the annulus is lower than inside the drill-string because the latter has a smaller cross-sectional area (except for slim hole and casing drilling which have very narrow annulus) [15]. Appropriate annular velocity has to be carefully optimized, because, annular velocity that is too high promotes hole erosion while too low causes inadequate cuttings transport.

2.5 Frictional Pressure Loss

As mentioned in section 2.2 and 2.3, there are many researches on the effects of drill-string tool joint and rotation on frictional pressure loss in the annulus. The effects of tool joint is significant on frictional pressure loss, which can be as high as 42% [18]. On the other hand, the effects of drill-string rotation on frictional pressure loss is more complex, depending on the fluid rheology. In this study, drilling mud with Power Law rheology (viscous and shear thinning fluid) will be used and according to the literature [7], [12], [21] the frictional pressure loss decreases with as rotation increases.

CHAPTER 3

3. METHODOLOGY

3.1 Computational Fluid Dynamics (CFD) Approach

This study employs Computational Fluid Dynamics (CFD) approach, using ANSYS-CFX as the simulation software, to investigate the hydraulic effects of drill-string tool joint and rotation on annular flow profile and frictional pressure loss. CFD approach is a well-established method to study and optimise fluid flow in different applications. Analytical solutions normally can only solve the simplest of fluid flow situations under ideal conditions. For this project, to obtain solutions for real flows, ANSYS-CFX, which adopts a numerical approach and uses algebraic approximations to solve nonlinear differential equations that govern the flow of fluid for predefined geometries and boundary conditions, i.e. conservation of mass, momentum and energy [1].

The assumptions of this study are: the power law (shear thinning) fluid is incompressible, the flow is steady state, fully developed and in isothermal condition. In Cartesian coordinates, the conservation equations of mass, momentum are expressed as [22]:

$$\frac{\partial \rho}{\partial t} + \frac{\partial}{\partial x_j} \cdot \left(\rho U_j\right) = 0 \tag{1}$$

$$\frac{\partial}{\partial t}\left(\rho U_i\right) + \frac{\partial}{\partial x_j} \cdot \left(\rho U_j U_i\right) = -\frac{\partial \mathrm{P}}{\partial x_i} + \frac{\partial}{\partial x_j}\left(\mu_{eff}\left(\frac{\partial U_i}{\partial x_j} + \frac{\partial U_j}{\partial x_i}\right)\right) \tag{2}$$

$$\frac{\partial}{\partial t}\left(\rho \varphi\right) + \frac{\partial}{\partial x_j} \cdot \left(\rho U_j \varphi\right) = \frac{\partial}{\partial x_j}\left(\Gamma_{eff}\left(\frac{\partial \varphi}{\partial x_j}\right)\right) + S_\varphi \tag{3}$$

In ANSYS-CFX, the governing equations are discretised using an element-based finite volume method, which dicretises the spatial domain using a mesh. The mesh is used to construct finite volumes. As explained by Ofei et al. [23], the discretised governing

equations, along with the initial and boundary conditions are solved for each finite volume in ANSYS-CFX solver.

Some advantages of CFD approach are: it provides realistic results based on physical governing equations, complex geometry can be simulated, costs much less than other approaches, consumes less time than physical experiments, and the results can be visualized.

3.2 ANSYS-CFX Work Flow

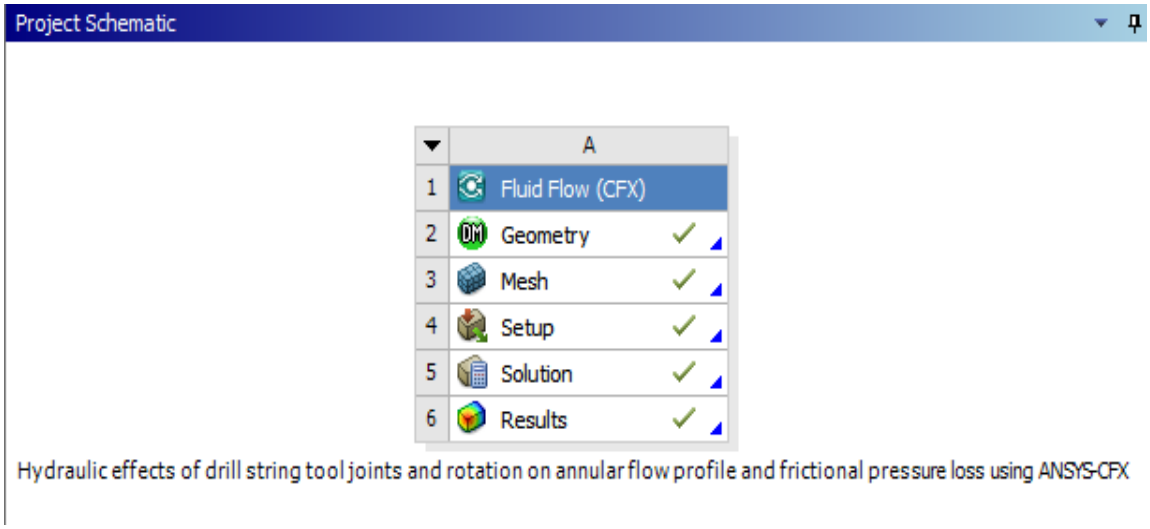

Figure 1: CFD project schematic in ANSYS Workbench under ANSYS-CFX analysis system

Figure 1 shows the entire project schematic in ANSYS-CFX, which consists of 5 successive elements, allowing us to sketch and build up the "geometry" (casing and drill pipe with tool joint), then discretise the geometry into tiny "meshes", and "setup" the physics and boundary conditions. Next, the simulation can be solved using the "solution" element and the results can be obtained in the "results" element. The 5 elements will be discussed in the following sections in details.

3.2.1 Geometry

In ANSYS 15 Workbench, under ANSYS-CFX analysis system, DesignModeler application is used for geometry modelling.

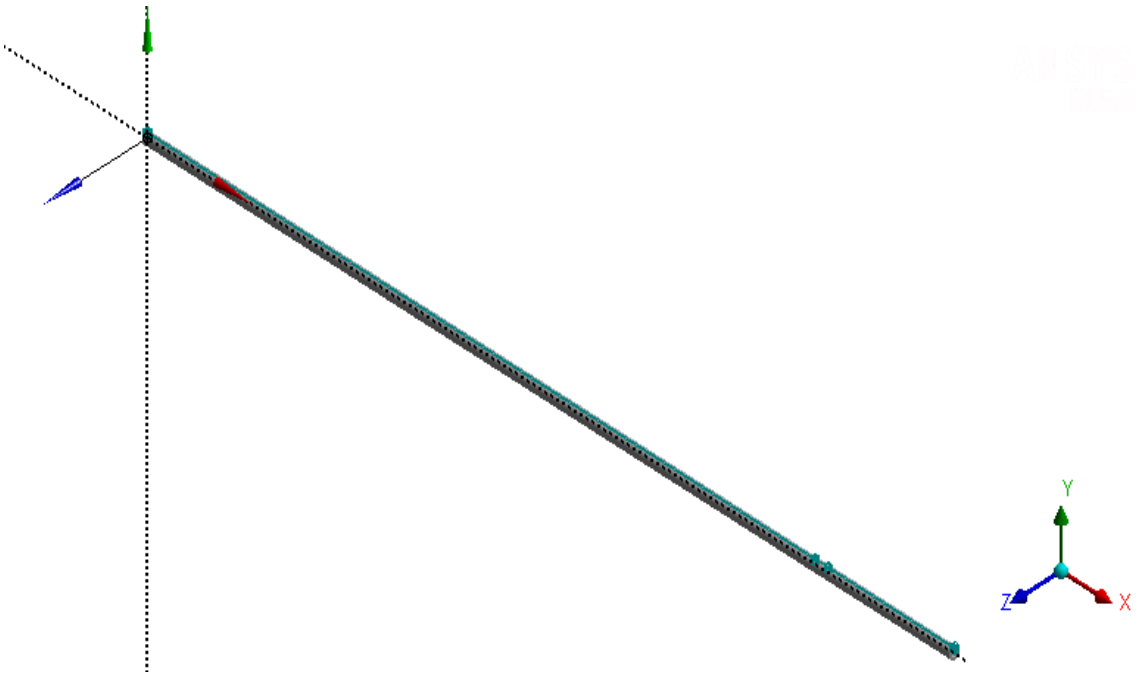

Figure 2: 3D view of CFD model geometry in DesignModeler

Figure 3: Close up view of CFD model geometry: Drill-string tool joint section

Figure 2 shows the 3D view of the geometry in DesignModeler application, whereas Figure 3 shows a closed up view of the drill-string tool joint (green) enclosed by the annulus space (grey).

Table 1 shows the general geometry of the CFD model that is applicable throughout this project. This project is divided into 3 main stages, and slightly different geometries are

used. The project stages are Grid Independence Study, Benchmarking and Design of Experiment.

Table 1: General geometry of the CFD model

	Inner Diameter, inch	Outer Diameter, inch	Length, ft
Casing	1.75	-	12.167
Drill pipe	-	1.25	12.167
Tool joint	-	1.50	0.2

The physical model consists of a horizontal wellbore which contains a drill-string (with 1 tool joint). The drill-string is concentric. This is illustrated in Figure 4.

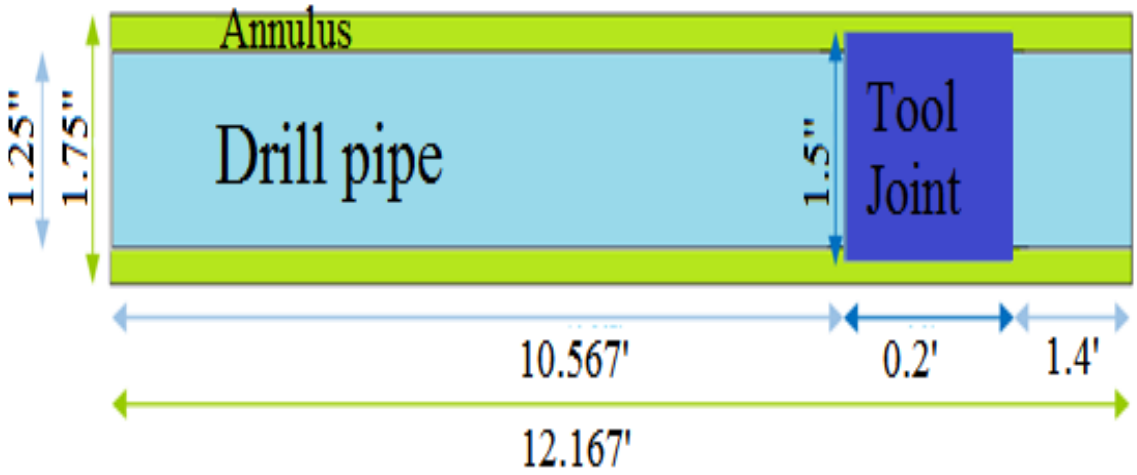

Figure 4: Physical model

On the other hand, for "Design of Experiment: case study based on design points" stage, the hydraulic effects of drill-string tool joint and rotation are studied. An identical horizontal wellbore which contains a drill-string is modelled. The drill-string is also concentric. Firstly, the drill-string is modelled without tool joint. Subsequently, one tool joint is added, similar to the previous stages.

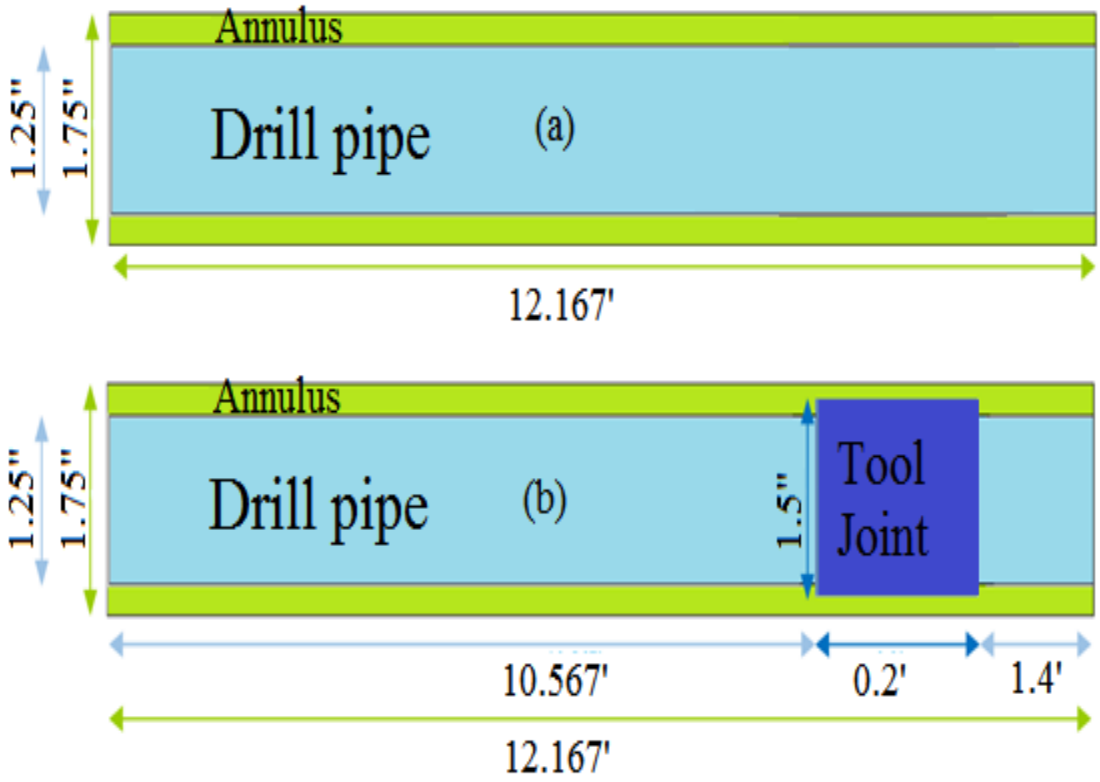

Figure 5: Geometry of the CFD model for "Design of Experiment: case study based on design points" stage (not-to-scale sketch)

In Figure 5, the upper geometry (a) is without tool joint while the lower geometry (b) is attached with a tool joint.

3.2.2 Mesh

The entire 3D wellbore, along with the drill-string in it, is discretised into unstructured tetrahedral mesh elements. Inflation layers are created near the walls covering about 20% of inner and outer radii for resolving the mesh in the near-wall region as well as accurately capturing the flow effects in that region.

In order to adjust the mesh size, body sizing option is inserted. This enables Grid Independence Study (section 3.3.1 Grid Independence Study) to be performed.

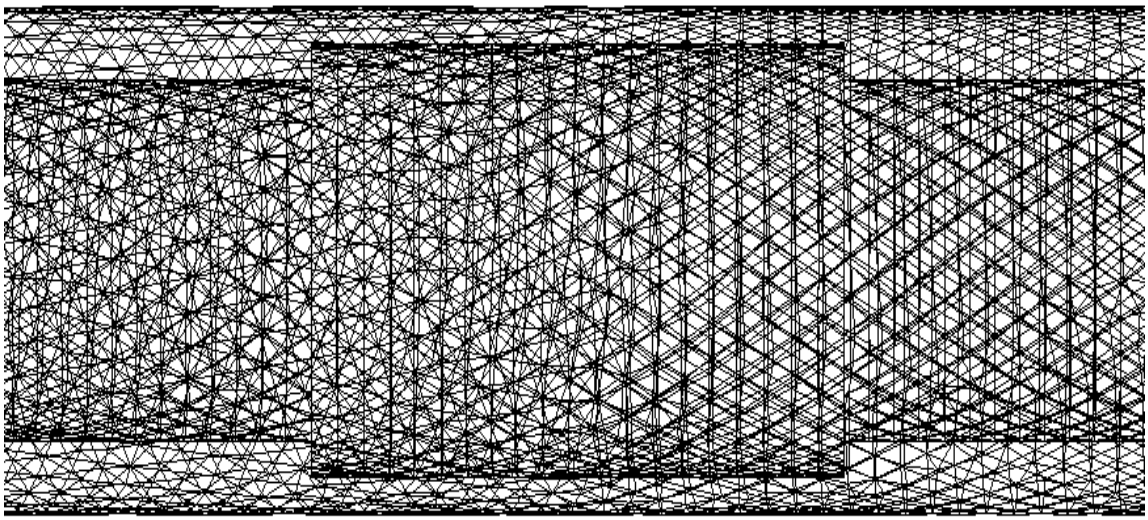

Figure 6: Meshing (longitudinal view)

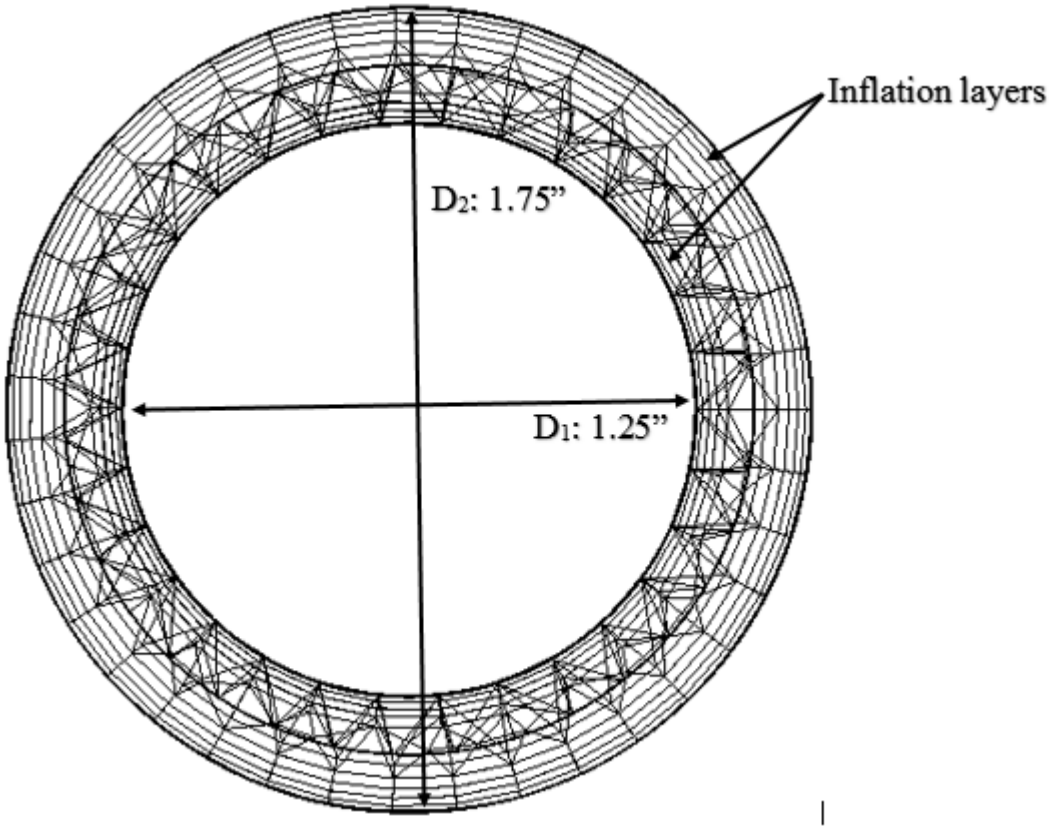

Figure 7: Meshing (cross-sectional view)

3.2.3 Setup: Physics And Boundary Conditions Modelling

Physics and boundary conditions can be modelled in "setup" using CFX-Pre application.

The physics of the CFD model includes assumptions such as steady state flow, isothermal condition and the fluid is incompressible.

For the inlet boundary condition, fluid velocity (ft/s) is the required input parameter, which is calculated from fluid flow rate (USgal/min) using the following equation:

$$v = \frac{q}{2.448(d_2{}^2 - d_1{}^2)} \quad (4)$$

Where v = fluid velocity (ft/s), q = fluid flow rate (USgal/min), d_2 = casing inner diameter (inch), d_1 = drill pipe outer diameter (inch).

Other boundary conditions are identical to a similar CFD research done by Ofei et al. [17]: zero gauge pressure is specified at the outlet. No slip boundary conditions were imposed on both inner and outer pipe wall for the fluid.

3.2.4 Solution: CFD Model Solving

Before solving the CFD model, the convergence criteria are defined in CFX-Pre, (1) the residual type is root mean square normalised value and (2) the residual target is 1 $x10^{-4}$. In this project, a maximum iterations of 100 is sufficient to achieve convergence, a higher value can be set if needed, however,in all cases, convergence is always achieved before the maximum number of iterations.

Using CFX-Solver Manager, the CFD simulation can be run.

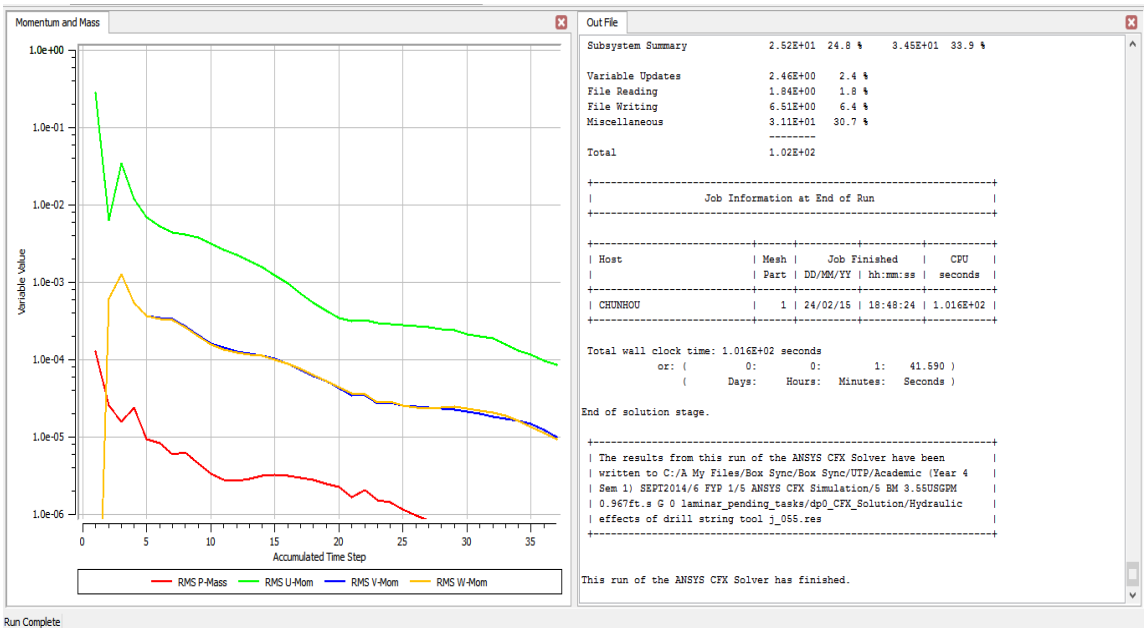

Figure 8: CFX-Solver Manager simulation monitor

As shown in Figure 8, the computation iterates until all variable values (momentum and mass) fall below the convergence criteria of 1E-4, which completes the simulation.

3.2.5 Results: Simulation Result Collection And Analysis

Upon completing the CFD simulation in ANSYS CFX, the simulation results can be obtained in CFD-Post in the form of spreadsheet, graph (Figure A-1.1) or visualisations. Visualisations include streamline (Figure A-1.2), contour (Figure A-1.3), volume rendering (Figure A-1.4) and etc.

Figure A-1.1 shows the graph of pressure distribution over the entire annulus length. The dramatic decrease in pressure indicates the location of the drill pipe tool joint (10.567 ft – 10.767 ft), which increases the pressure loss by decreasing the annulus cross-sectional area.

3.3 Main Project Stages

3.3.1 Grid Independence Study

The smaller the mesh size, the more accurate is the CFD simulation result, but the longer is the CFD simulation time. Grid independence study is carried out with the objective of determining the optimum mesh size, which will result in a simulation time that still yields similar results, as compared to smaller mesh sizes.

During the grid independence study, different mesh element sizes are investigated, ranging from 0.008 ft to 0.015 ft. As mentioned in section 3.2.2, body sizing option is used to adjust the mesh element size.

Table 2: Number of mesh element used in grid independence study

Mesh element size (ft)
0.008
0.010
0.012
0.013
0.015

Simulation is run with Power Law fluid E flowing at 3 USgal/min, the tool joint is present and the drill-string is not rotating (0 RPM). The resulting pressure loss across the 36" (3') tool joint section was obtained. Different mesh element sizes produced different values of pressure loss. When the pressure loss trend is stable, the biggest mesh element size is considered as the optimum mesh.

Table 3: Grid independence study (table)

Upstream pressure (at 9.167ft) (psi)	Downstream pressure (at 12.167ft) (psi)	Pressure drop (psi)	Mesh element size (ft)	Remark
0.851620	0.00	0.851620	0.008	
0.851620	0.00	0.851620	0.010	
0.851620	0.00	0.851620	0.012	Optimum
0.810640	0.00	0.810640	0.013	
0.802801	0.00	0.802801	0.015	

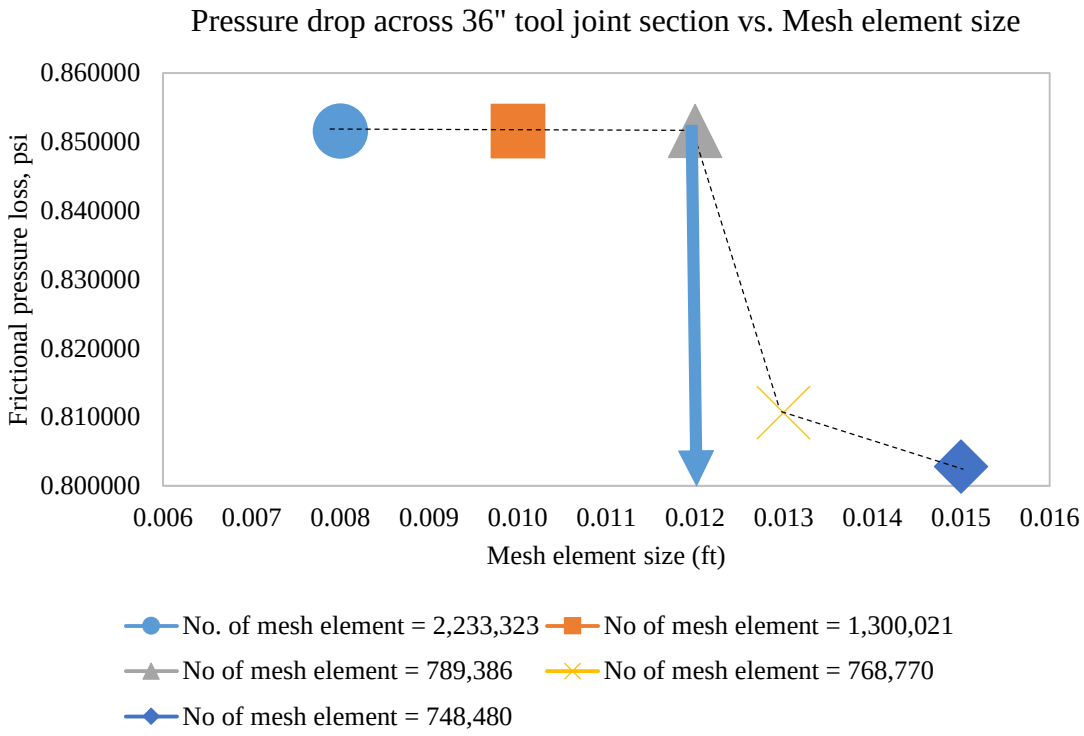

Figure 9: Grid independence study (graph)

Table 3 and Figure 9 show the result of grid independence study. The plot shows a constant 0.851620 psi pressure loss from 0.008 – 0.012 ft mesh element sizes. Mesh element sizes larger than 0.012 ft yield different pressure loss values. Therefore, it can be concluded that 0.012 ft is the optimum mesh element size that would minimise simulation time and yet yield similar result, as compared to the smaller mesh element sizes.

3.3.2 Benchmarking: CFD Model Validation With Experimental Data

For this project, the benchmark is based on the experiment carried out by Enfis [24]. The simulation results will be compared with the experimental results in order to validate the CFD model.

Enfis carried out experiments using Power Law fluids, labeled as fluid E and fluid G,. The properties of the Power Law fluids are tabulated as shown in Table 4.

Table 4: Power Law Fluids Properties

Power law fluids		
Fluid	E	G
Density (lbm/ft^3)	62.3	62.5
k, flow consistency index ($lbf. S^n/ft^2$)	0.01	0.0466
n, flow behavior index	0.6120	0.4097

The experiment consists of three different series of frictional pressure loss readings across three different locations along the drill-string:

- P1 (36" tool joint section, 9.167ft – 12.167 ft)
- P2 (12" section without tool joint, 8 ft – 9 ft)
- P3 (12" tool joint section, 10.167 ft – 11.167 ft)

In the course of benchmarking, many adjustments were made to the geometry and CFD model physics and boundary conditions, in order to improve the match between CFD simulation results and the experimental data. Table A-2.1shows the adjustments and their effects on the benchmarking. Problems in Table A-2.1, adjustments that are marked with √ helped to improve the match between CFD simulation results and experimental data. Therefore, they were taken into considerations.

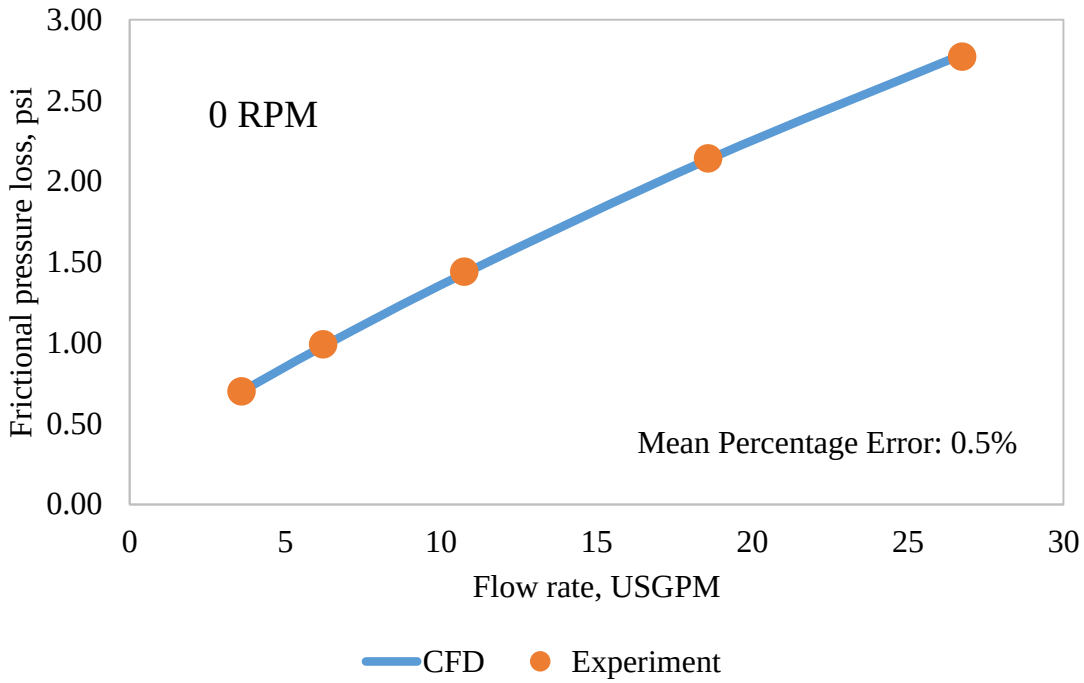

Figure 10: Frictional pressure loss between CFD simulation and experimental results for fluid E at P1: 36" tool joint section

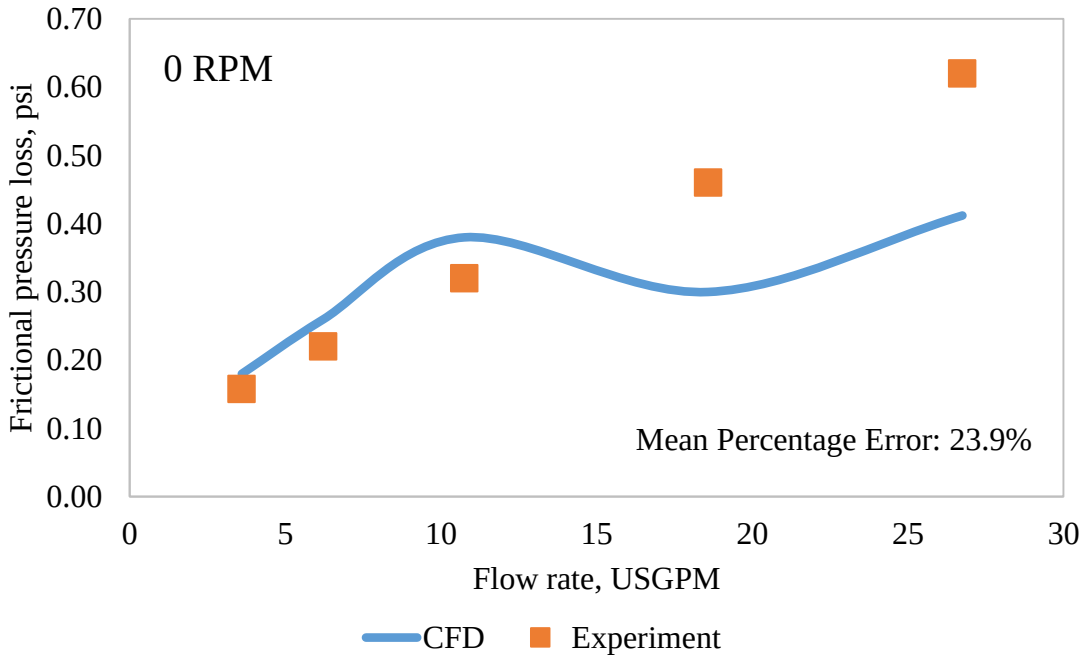

Figure 11: Frictional pressure loss between CFD simulation and experimental results for fluid E at P2: 12" section without tool joint

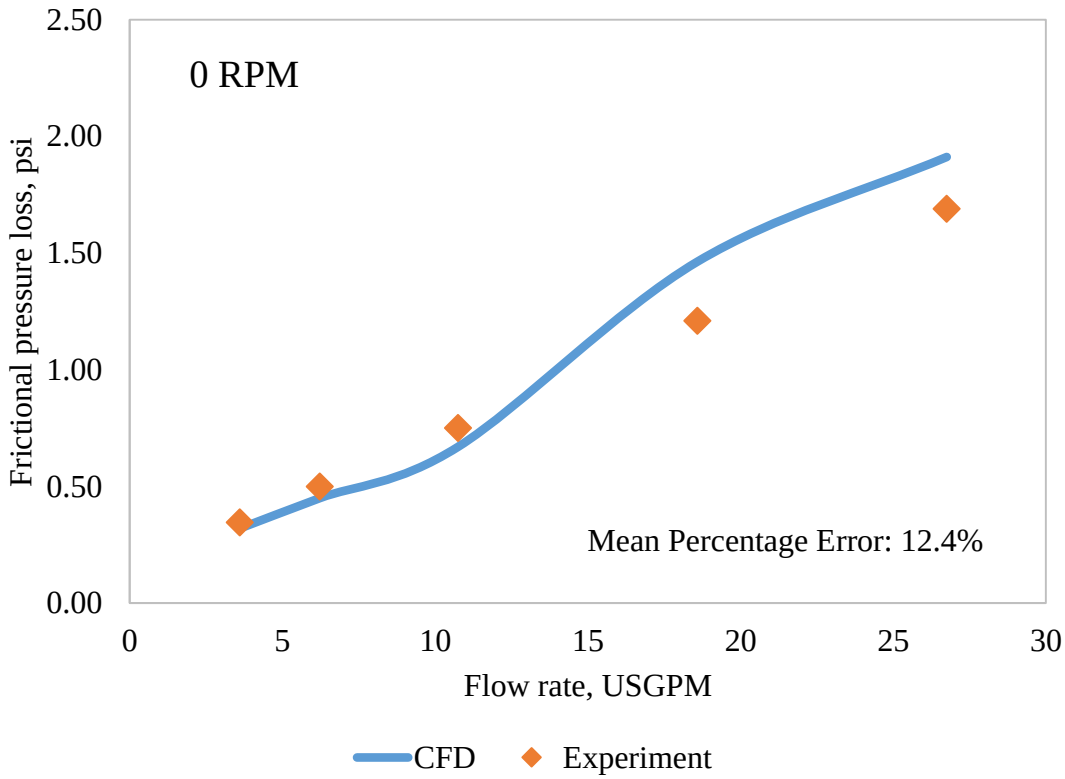

Figure 12: Frictional pressure loss between CFD simulation and experimental results for fluid E at P3: 12" tool joint section

Table A-3.1 to Table A-3.3 and Figure 10 to Figure 12 show pressure loss values (P1, P2, and P3) versus flow rates, with both CFD simulation result and experimental result. We can observe that the pressure loss magnitude is the highest in the 36" tool joint section, followed by 12" tool joint section and the smallest pressure loss occurs in the 12" section without tool joint. Both experimental and CFD simulation results show similar pressure loss readings, with mean percentage error from 0.5% to 23.9%.

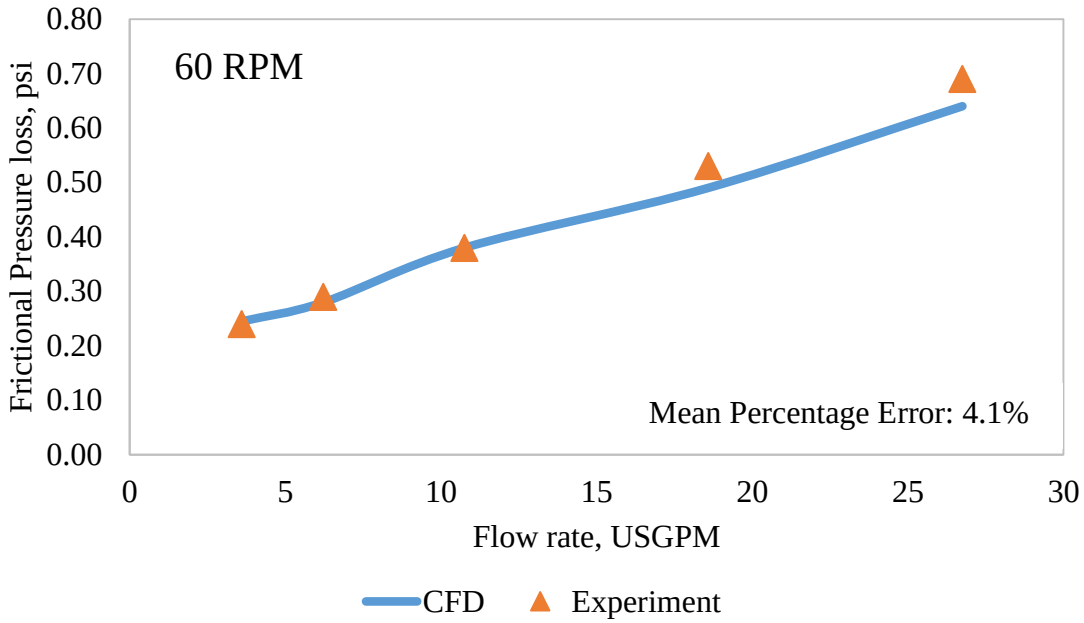

Figure 13: Frictional pressure loss between CFD simulation and experimental results for fluid G at P2: 12" section without tool joint

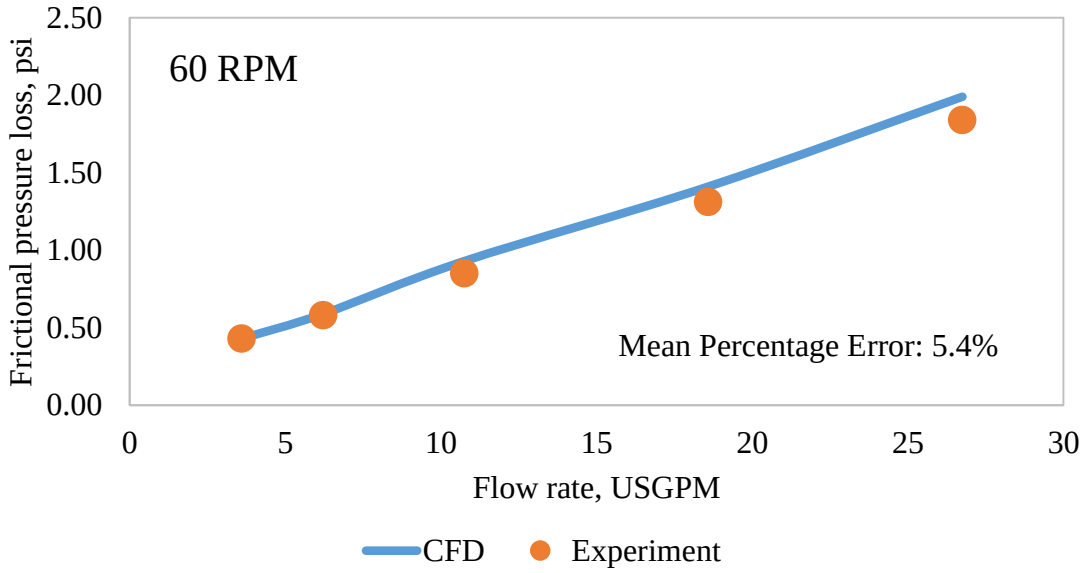

Figure 14: Frictional pressure loss between CFD simulation and experimental results for fluid G at P3: 12" tool joint section

Table A-3.4, Table A-3.5, Figure 13 and Figure 14 show pressure loss values (P2 and P3) versus flow rates for 60 RPM drill-string rotation speed, with both CFD simulation result and experimental result. Both experimental and CFD simulation results show similar pressure loss readings (P2 and P3), with mean percentage error of 4.1% and 5.4%.

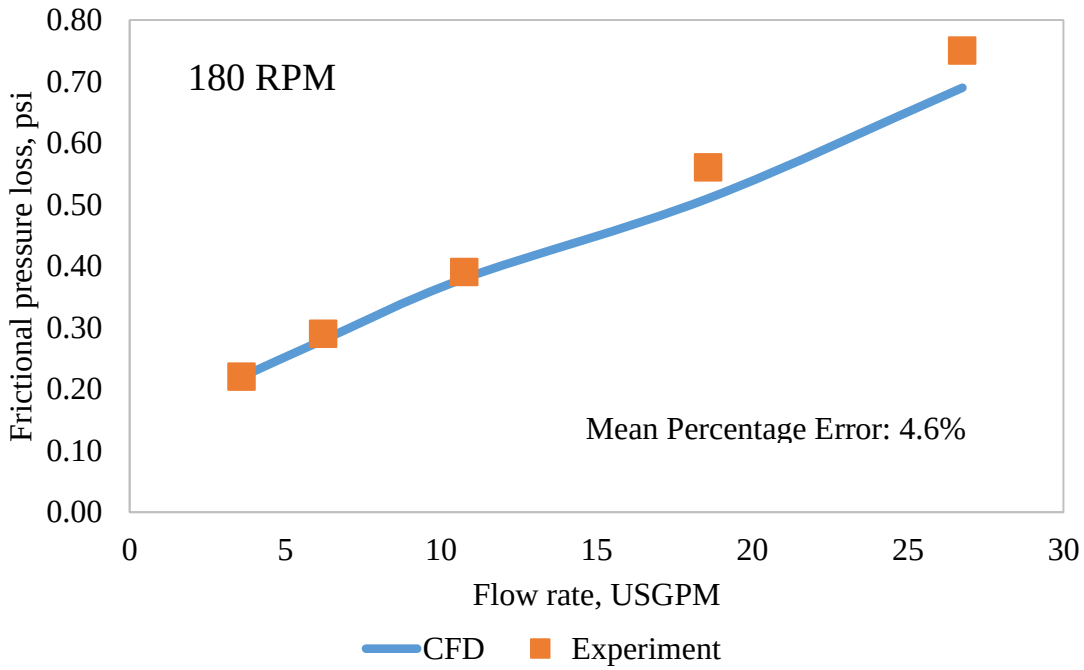

Figure 15: Frictional pressure loss values between CFD simulation and experimental results for fluid G at P2: 12" section without tool joint

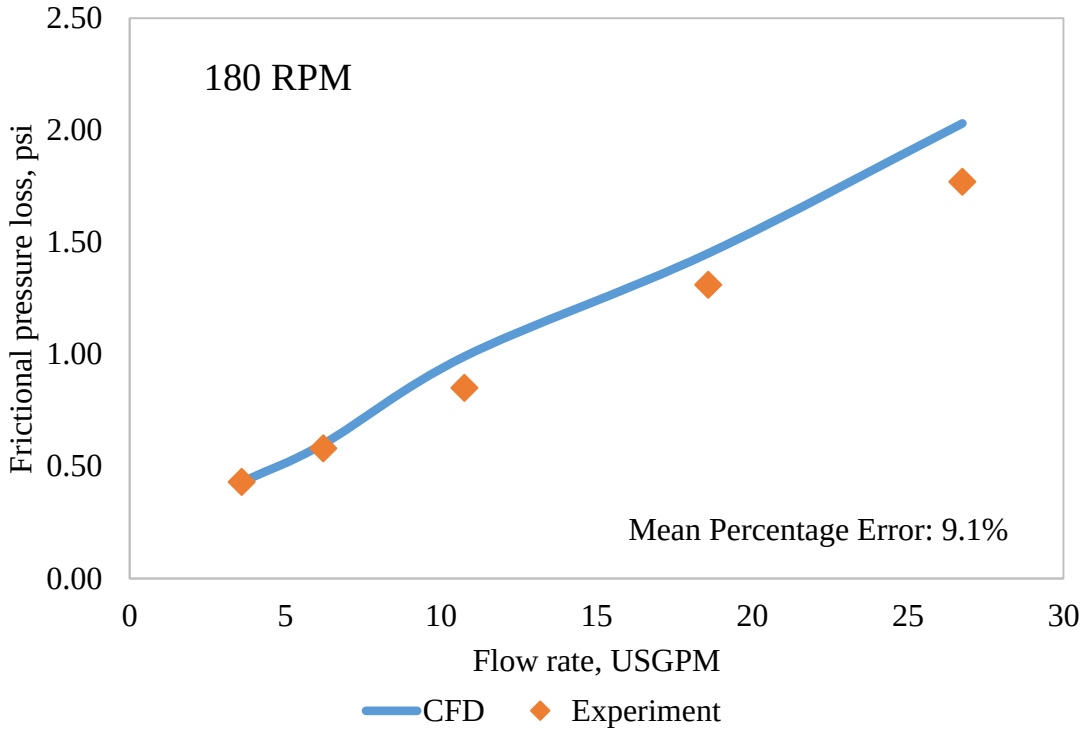

Figure 16: Frictional pressure loss values between CFD simulation and experimental results for fluid G at P3: 12" tool joint section

Table A-3.4, Table A-3.5, Figure 15 and Figure 16 show pressure loss values (P2 and P3) versus flow rates for 180 RPM drill-string rotation speed, with both CFD simulation result

and experimental result. Both experimental and CFD simulation results show similar pressure loss readings (P2 and P3), with mean percentage error of 4.6% and 9.1%.

3.3.3 Design of Experiment: Case Study Based On Design Points

Once the CFD model has been validated, a process known as "Design of Experiment" [25] is used to create a case study that investigates important factors or design points that would have higher impact on the responses of this project, i.e. annular flow profile and frictional pressure loss.

Table 5: Design of Experiment

Factors		Responses
Drill-string rotation (RPM)	Number of tool joint	
0	0	Velocity Dynamic viscosity Frictional pressure loss
	1	
	2	
60	0	
	1	
120	0	
	1	
180	0	
	1	
240	0	
	1	
300	0	
	1	
420	0	
	1	
540	0	
	1	
600	0	
	1	

The results will provide insights for the design of drilling hydraulics and optimise drilling operation in narrow drilling margin or slimhole wells.

3.4 Project Key Milestones

Table 6: Project Key Milestones

Project Key Milestones		Date
FYP 1	Project topic selection	September 22 - September 28, 2014
	Literature review	September 29 - October 12, 2014
	ANSYS CFX learning	October 13 - October 26, 2014
	CFD project file setup	October 27 - October 31, 2014
	Geometry modelling	November 1 - November 7, 2014
	Meshing	November 8 - November 21, 2014
	Grid independence study	November 22 - December 5, 2014
	Physics and boundary conditions modeling	December 6 - December 12, 2014
	CFD Model Solving	December 13 - December 19, 2014
	Simulation result collection and analysis	December 20 - December 26, 2014
FYP 2	Benchmarking: Adjust physics and boundary conditions	January 12 – January 26, 2015
	Benchmarking: CFD model validation with experimental data (w/o rotation)	January 27 - February 5, 2015
	Benchmarking: CFD model validation with experimental data (with rotation)	February 6 - February 15, 2015
	Design of Experiment: Case study based on design points	February 16 – March 19, 2015
	Further parametric study	March 20 – April 20, 2015

3.5 Project Timeline – Gantt Chart

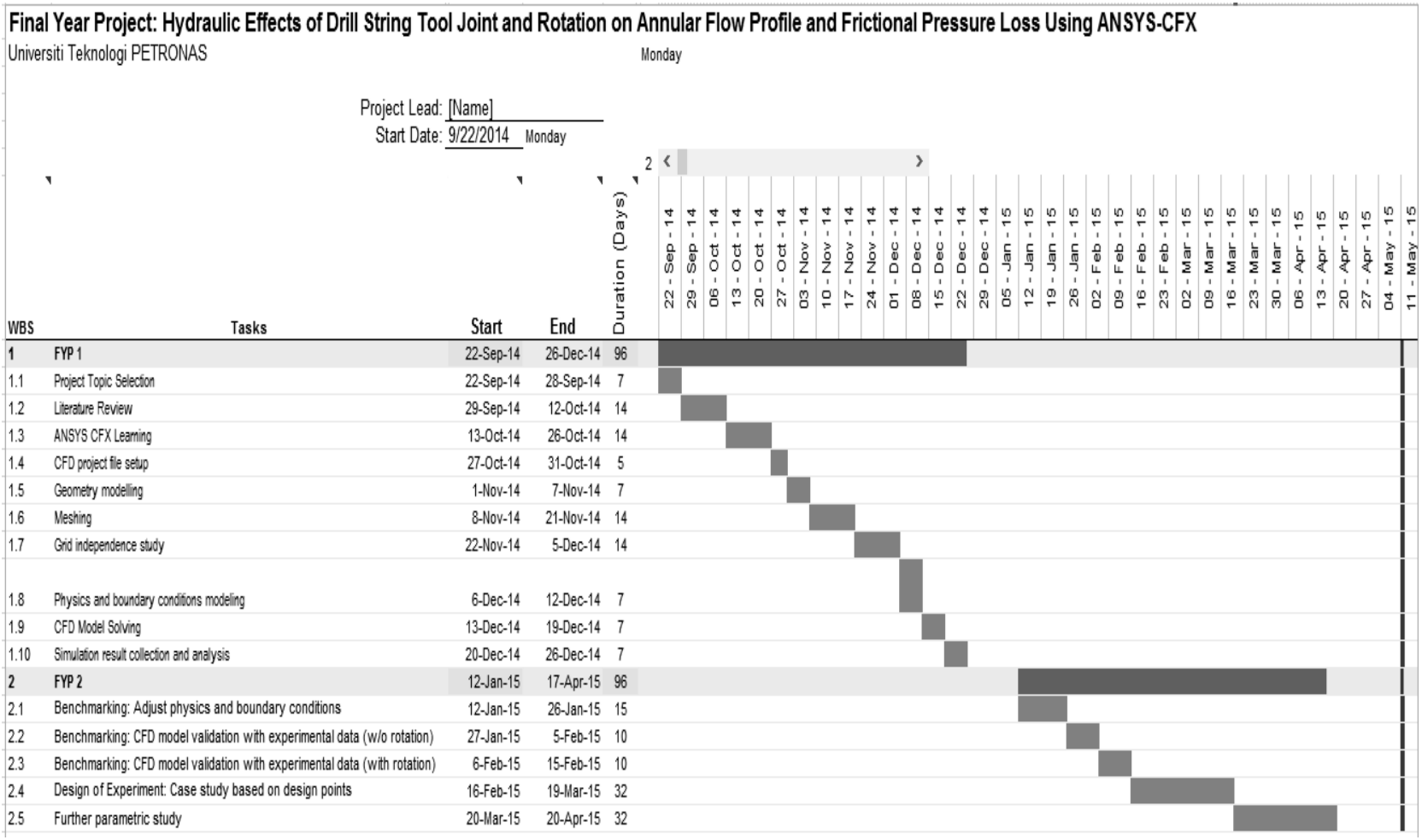

WBS	Tasks	Start	End	Duration (Days)
1	FYP 1	22-Sep-14	26-Dec-14	96
1.1	Project Topic Selection	22-Sep-14	28-Sep-14	7
1.2	Literature Review	29-Sep-14	12-Oct-14	14
1.3	ANSYS CFX Learning	13-Oct-14	26-Oct-14	14
1.4	CFD project file setup	27-Oct-14	31-Oct-14	5
1.5	Geometry modelling	1-Nov-14	7-Nov-14	7
1.6	Meshing	8-Nov-14	21-Nov-14	14
1.7	Grid independence study	22-Nov-14	5-Dec-14	14
1.8	Physics and boundary conditions modeling	6-Dec-14	12-Dec-14	7
1.9	CFD Model Solving	13-Dec-14	19-Dec-14	7
1.10	Simulation result collection and analysis	20-Dec-14	26-Dec-14	7
2	FYP 2	12-Jan-15	17-Apr-15	96
2.1	Benchmarking: Adjust physics and boundary conditions	12-Jan-15	26-Jan-15	15
2.2	Benchmarking: CFD model validation with experimental data (w/o rotation)	27-Jan-15	5-Feb-15	10
2.3	Benchmarking: CFD model validation with experimental data (with rotation)	6-Feb-15	15-Feb-15	10
2.4	Design of Experiment: Case study based on design points	16-Feb-15	19-Mar-15	32
2.5	Further parametric study	20-Mar-15	20-Apr-15	32

Figure 17: Gantt Chart

3.6 Simulation Flow Chart

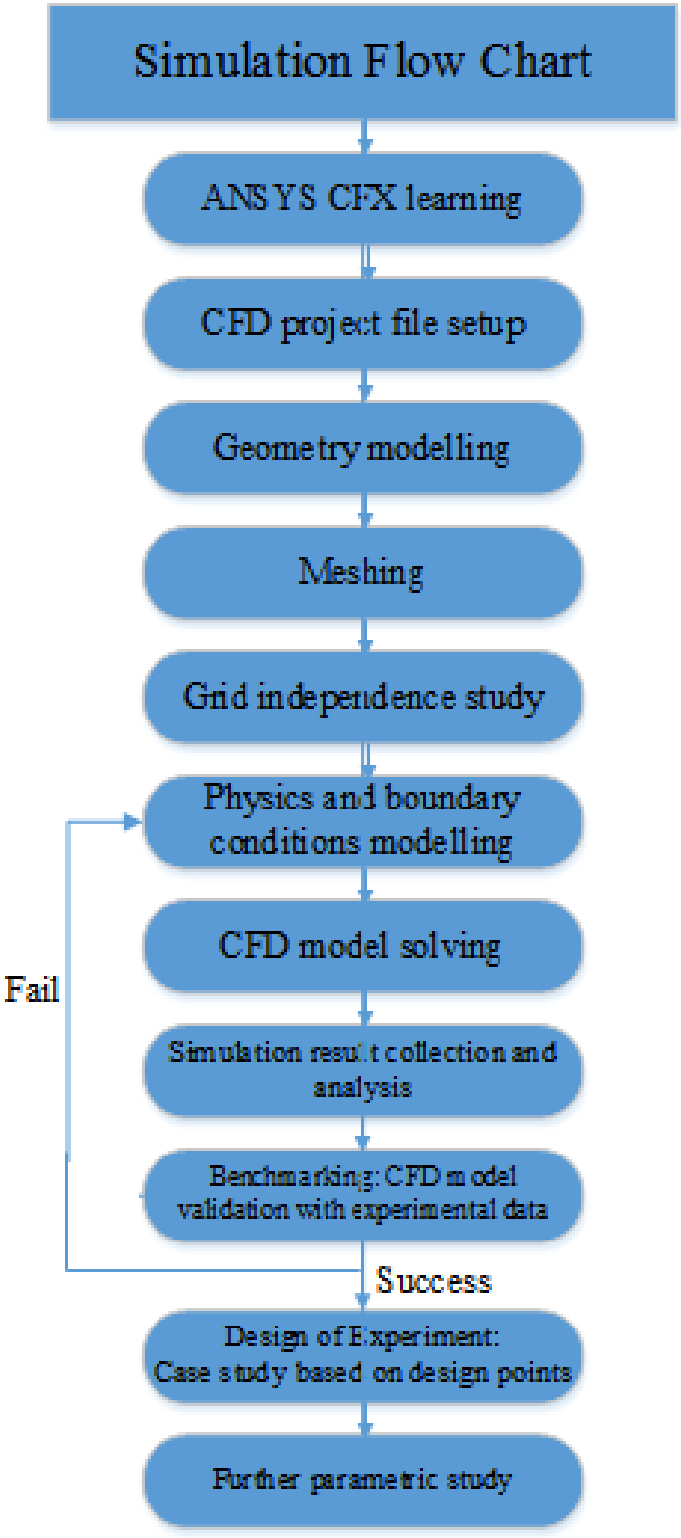

Figure 18: Simulation flow chart

CHAPTER 4

4. RESULT AND DISCUSSION

In this chapter, Design of Experiment was used to carry out case studies which investigated the important factors that affect the responses, as documented in Table 5.

4.1 Hydraulic Effects of Drill-String Tool Joint on Annular Flow Profile and Frictional Pressure Loss

Firstly, the hydraulic effects of drill-string tool joint on annular flow profile and frictional pressure loss were investigated. The number of tool joint ranged from 0, 1 to 2. In this case, the drill-string rotation speed was maintained at 0 RPM.

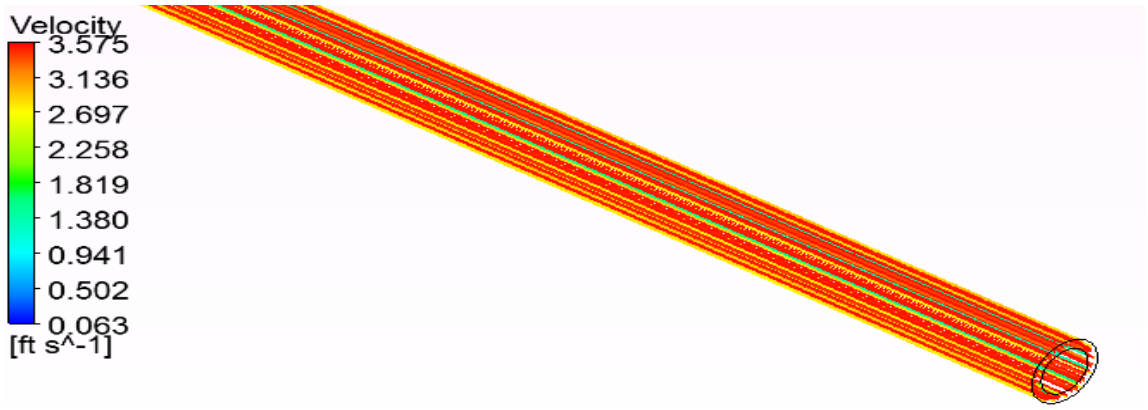

Figure 19: Annular flow profile without tool joint

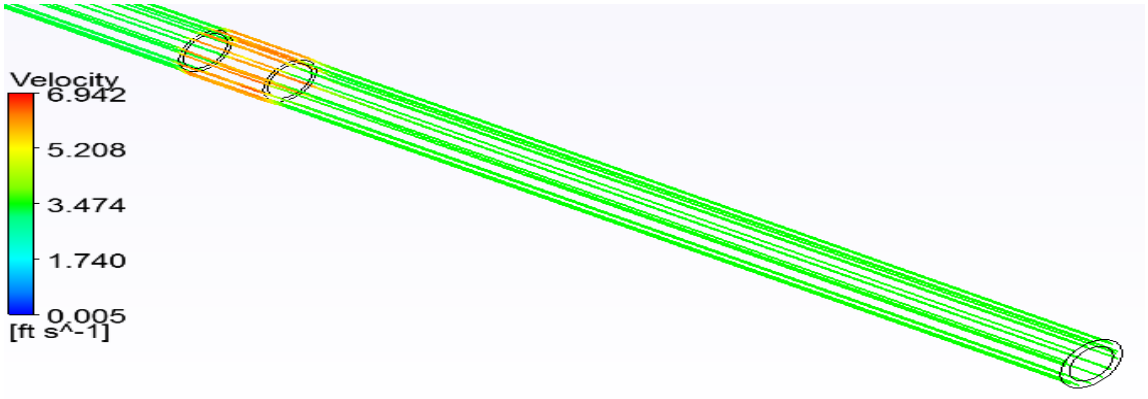

Figure 20: Annular flow profile with 1 tool joint

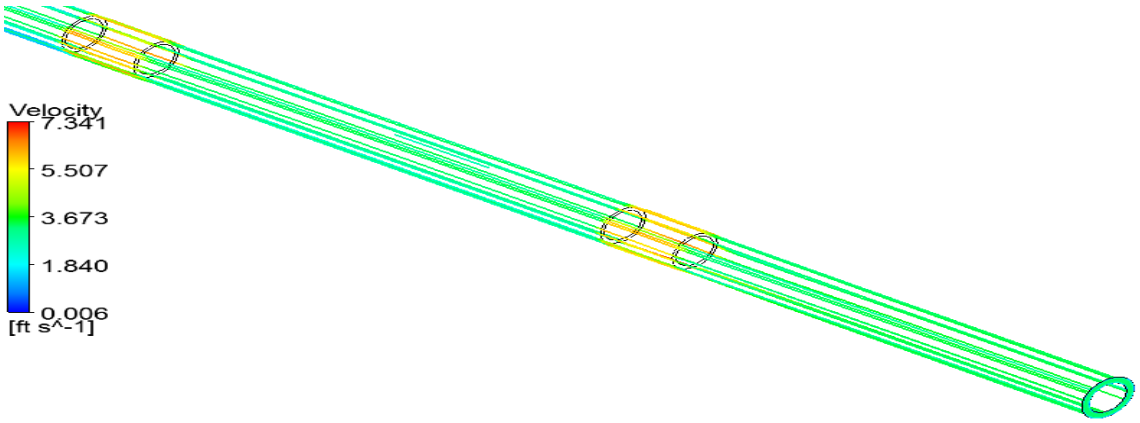

Figure 21: Annular flow profile with 2 tool joints

Figure 19 to Figure 21 present the influence of tool joint on the annular flow profile. It is observed that around the tool joint section(s), the fluid velocity is higher than the rest of the annulus. In Figure 19 (without tool joint), the fluid velocity appears to be uniform and peaks at 3.575 ft/s. In Figure 20 (1 tool joint), the peak fluid velocity is 6.776 ft/s, at the tool joint section. Lastly, in Figure 21 (2 tool joints), the peak fluid velocity is at 7.341 ft/s, at the tool joint sections.

Hence, there is an increasing trend in the peak fluid velocity as the number of tool joint increases.

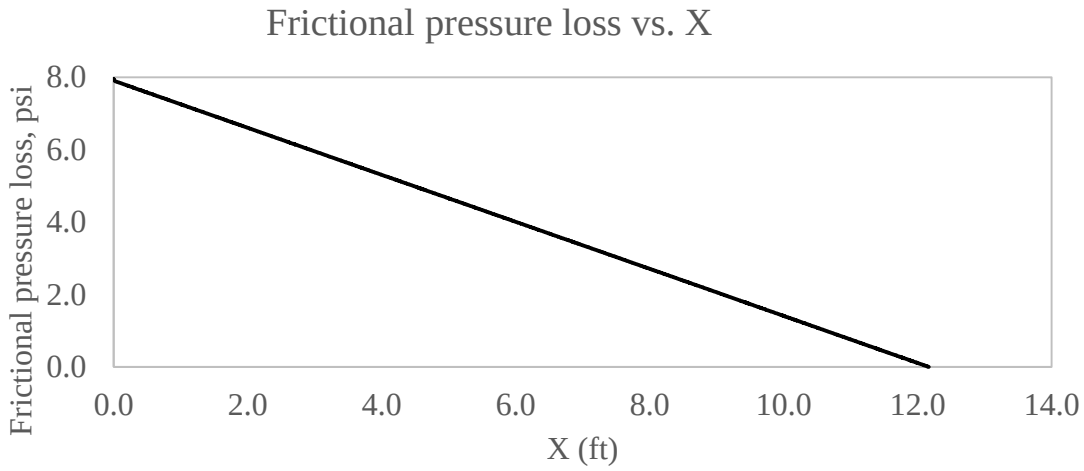

Figure 22: Frictional pressure loss along the annulus at 0 RPM with no tool joint

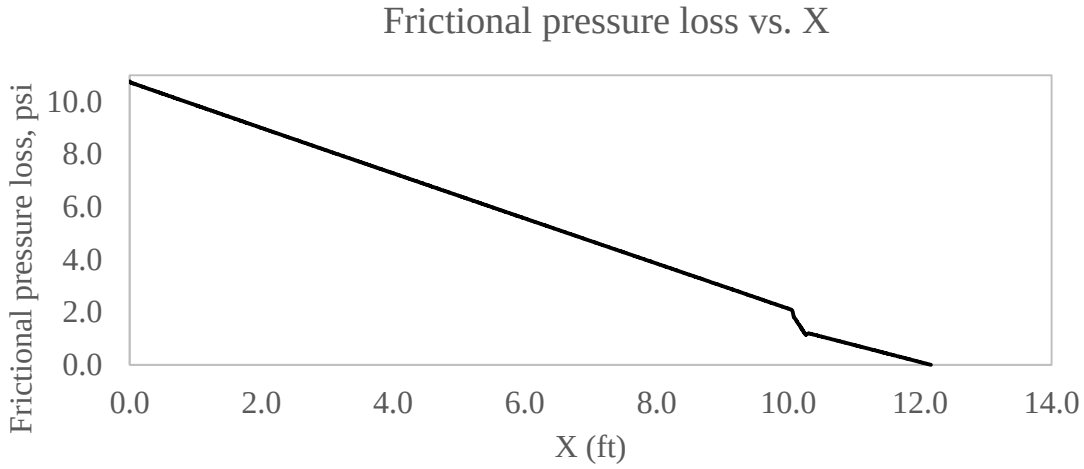

Figure 23: Frictional pressure loss along the annulus at 0 RPM with 1 tool joint

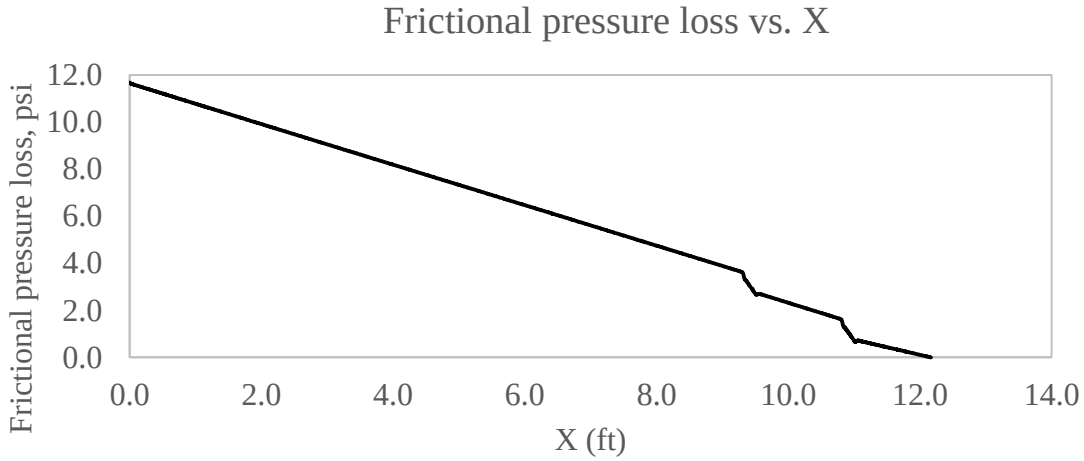

Figure 24: Frictional pressure loss along the annulus at 0 RPM with 2 tool joints

Figure 22 to Figure 24 show the frictional pressure loss along the annulus as the number of tool joint increases from 0 to 2. In Figure 22, the frictional pressure loss is gradual and smooth, because there is no tool joint, hence the annular space has a uniform dimension. However, in Figure 23 and Figure 24, the slope of the plots dramatically changes at the tool joint section, because the annular space decreases with the presence of tool joint(s), hence increasing the amount of frictional pressure loss.

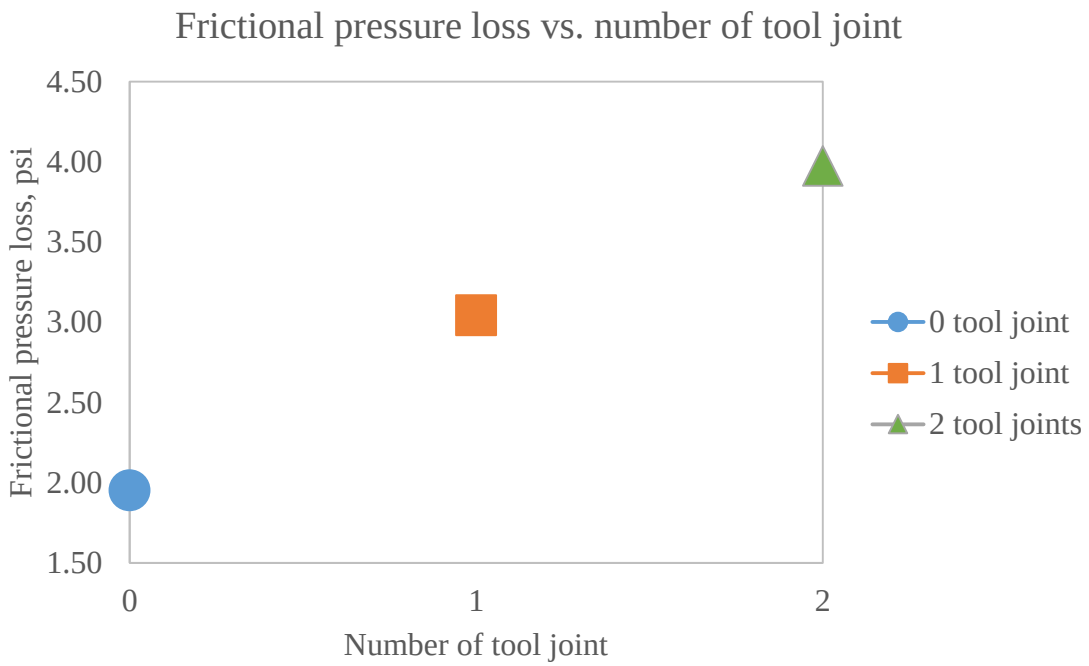

Figure 25: Pressure loss versus number of tool joint at 0 RPM drill-string rotation speed

From Table A-4.1 and Figure 25, we can observe that as the number of tool joint increases, the frictional pressure loss increases from 1.953 psi (no tool joint) to 3.044 psi (1 tool joint) and then 3.976 psi (2 tool joints), which translates into a 55.9% increase in frictional pressure loss from no tool joint to 1 tool joint;.

The higher the number of tool joint, the higher the frictional pressure loss.

4.2 Hydraulic Effects of Drill-String Rotation on Annular Flow Profile and Frictional Pressure Loss

Secondly, the hydraulic effects of drill-string rotation on annular flow profile and frictional pressure loss were investigated. The drill-string rotation speed ranged from 0 to 600 RPM. In this case, there is no drill-string tool joint.

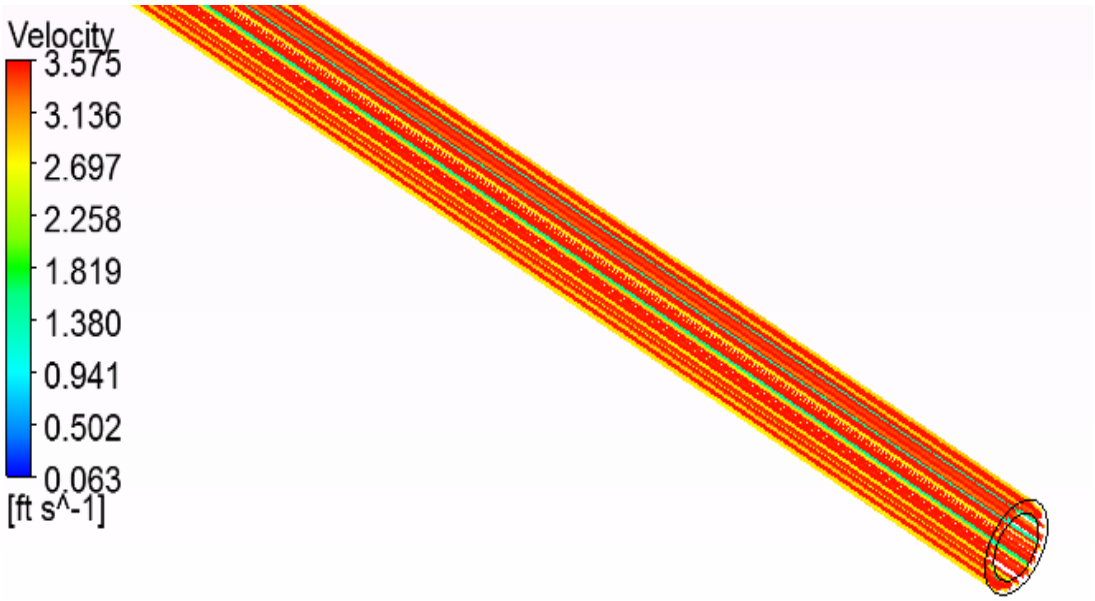

Figure 26: Annular flow profile at 0 RPM without tool joint

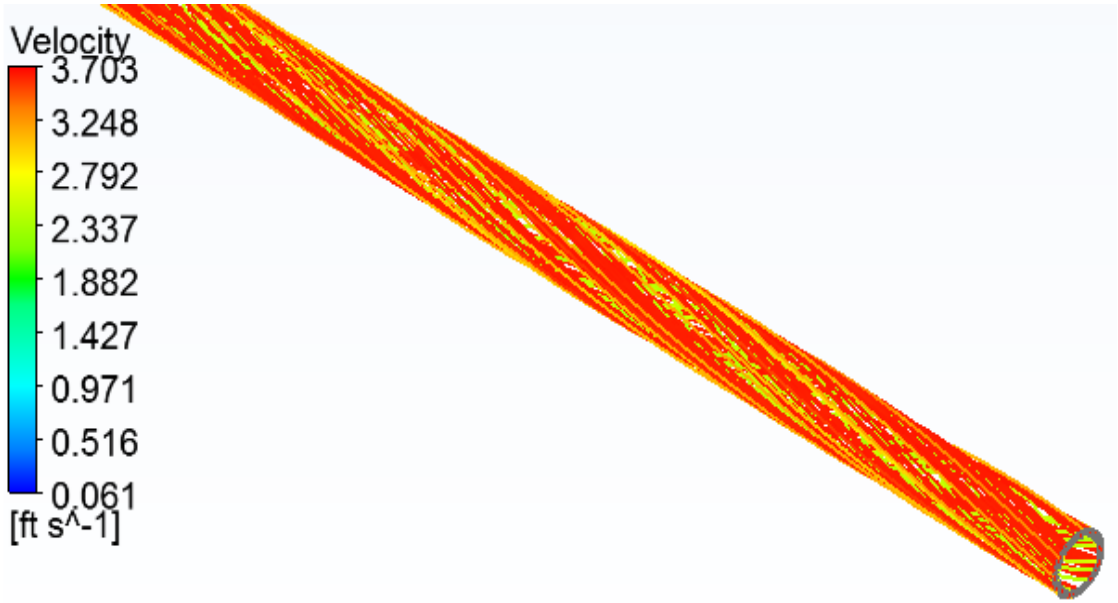

Figure 27: Annular flow profile at 300 RPM without tool joint

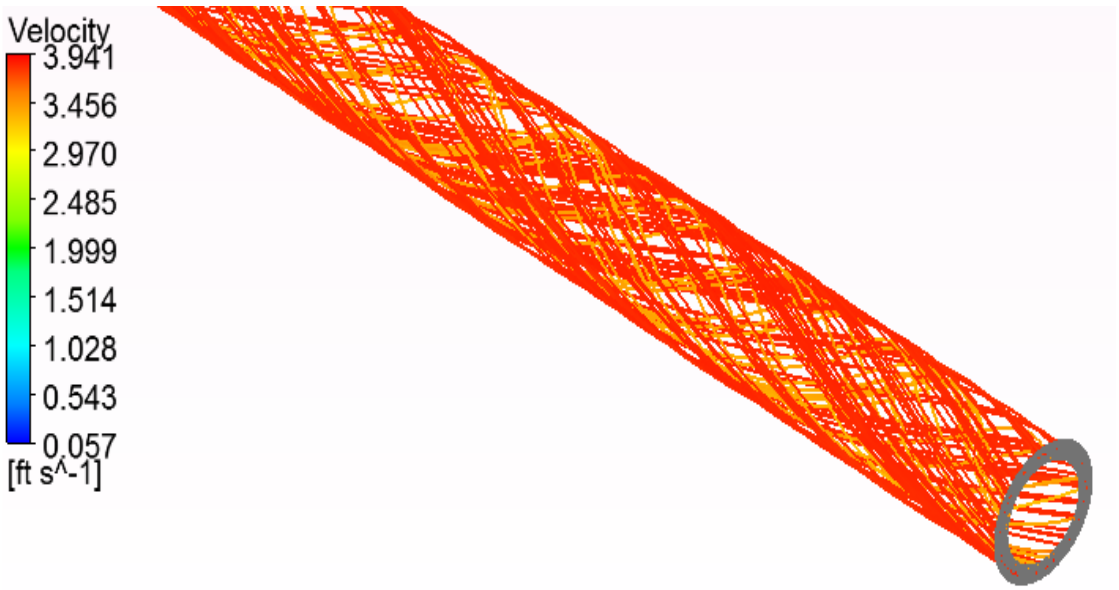

Figure 28: Annular flow profile at 600 RPM without tool joint

Figure 26 to Figure 28 present the influence of drill-string rotation speed on the annular flow profile. It is observed that as the rotation speed increases, the fluid velocity increases. In Figure 26, at 0 RPM, the peak fluid velocity is 3.575 ft/s. In Figure 28, at 600 RPM, the peak fluid velocity increases to 3.941 ft/s.

There is an increasing trend in the peak fluid velocity as drill-string rotation speed increases.

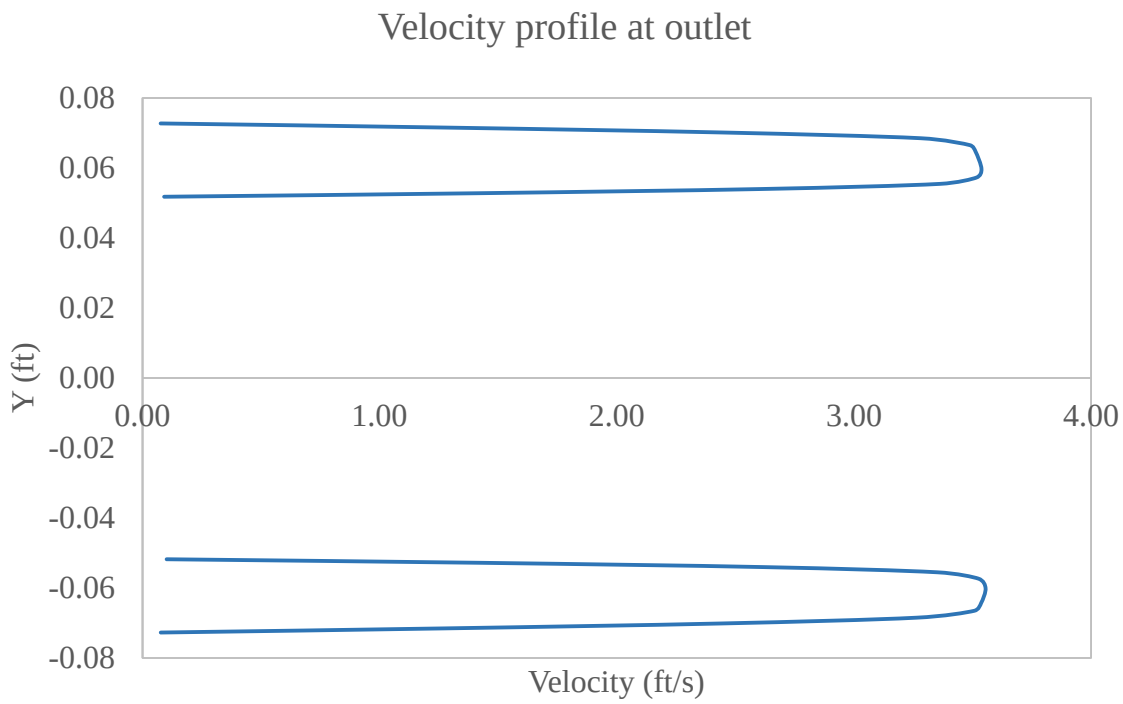

Figure 29: Velocity profile at the outlet at 0 RPM without tool joint

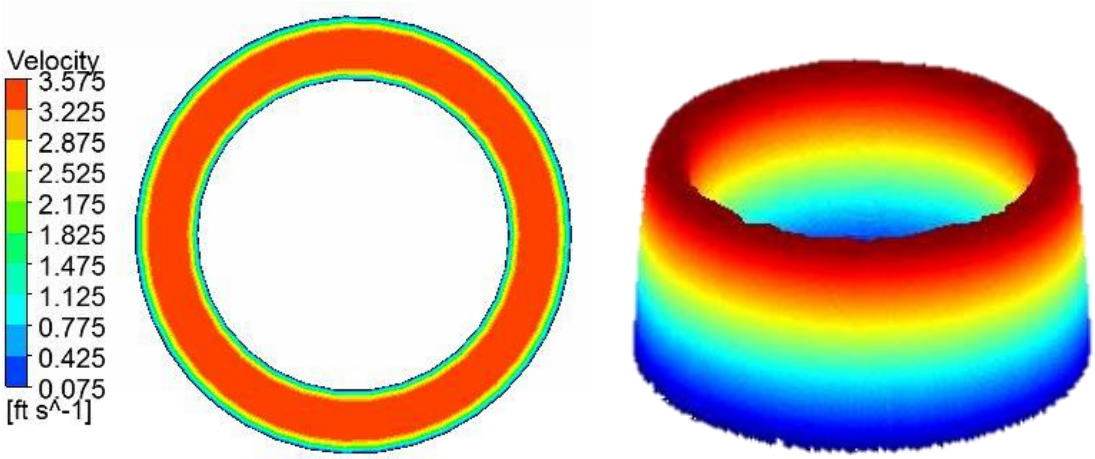

Figure 30: 2D (left) and 3D (right) velocity profile at the outlet at 0 RPM without tool joint

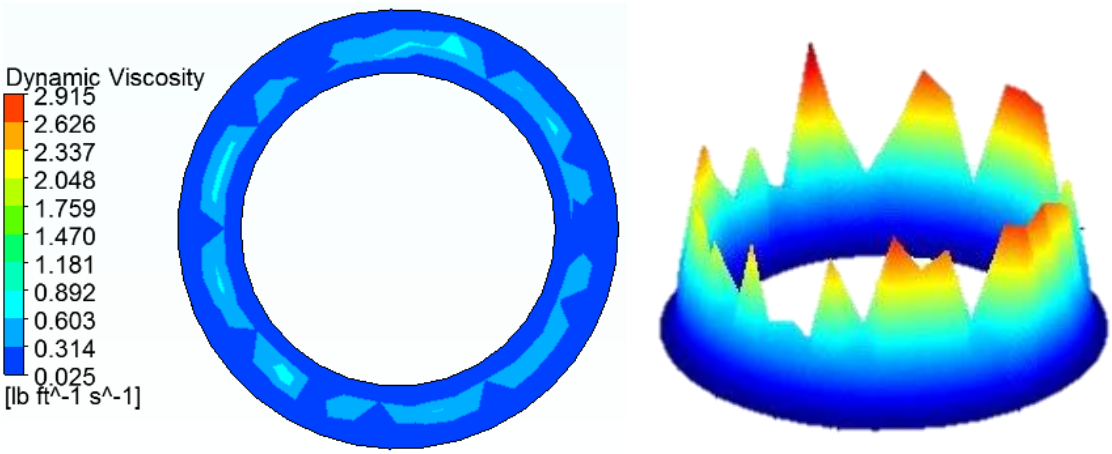

Figure 31: 2D (left) and 3D (right) dynamic viscosity profile at the outlet at 0 RPM without tool joint

At drill-string rotation speed of 0 RPM, the velocity profile at the outlet is plotted in Figure 29, and shown in both 2D and 3D in Figure 30. On the other hand, Figure 31 shows the 2D and 3D dynamic viscosity profile.

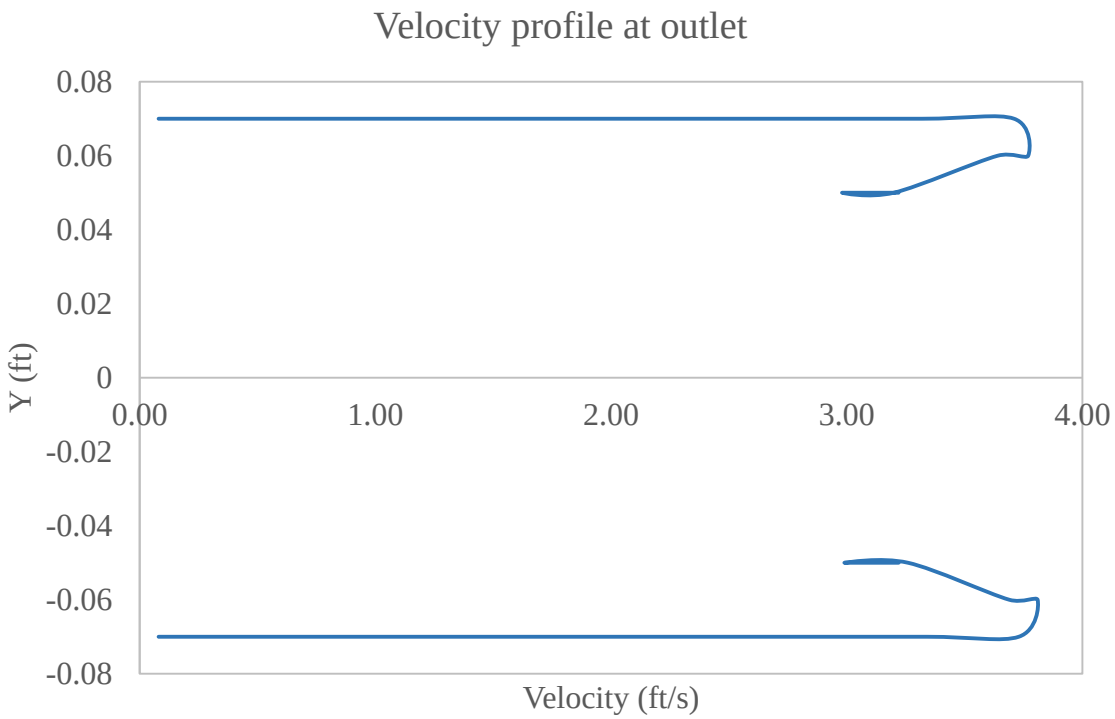

Figure 32: Velocity profile at the outlet at 600 RPM without tool joint

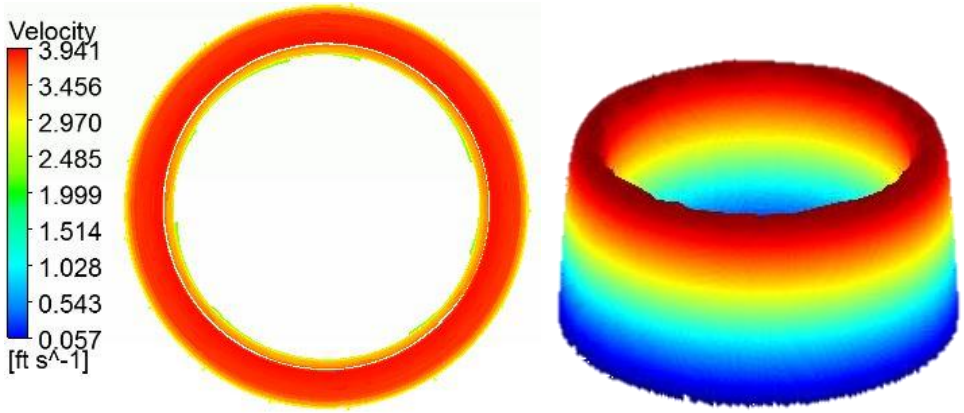

Figure 33: 2D (left) and 3D (right) velocity profile at the outlet at 600 RPM without tool joint

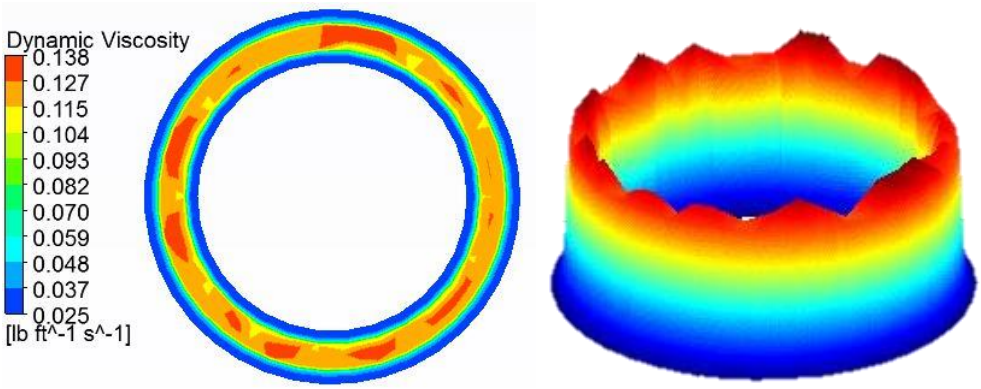

Figure 34: 2D (left) and 3D (right) dynamic viscosity profile at the outlet at 600 RPM without tool joint

At drill-string rotation speed of 600 RPM, the velocity profile at the outlet is plotted in Figure 32, and shown in both 2D and 3D in Figure 33. On the other hand, Figure 34 shows the 2D and 3D dynamic viscosity profile.

Comparing the outlet velocity profiles of 0 RPM and 600 RPM, it can be observed that drill-string rotation increases the fluid velocity near the drill-string outer wall by 98.4%. Without drill-string rotation, the fluid near the drill-string outer wall is almost static.

On the other hand, comparing the outlet dynamic viscosity profiles of 0 RPM and 600 RPM, it can be observed that drill-string rotation decreases the fluid dynamic viscosity, because of the increased fluid velocity. Without drill-string rotation, the fluid dynamic viscosity is higher, due to a slower fluid velocity.

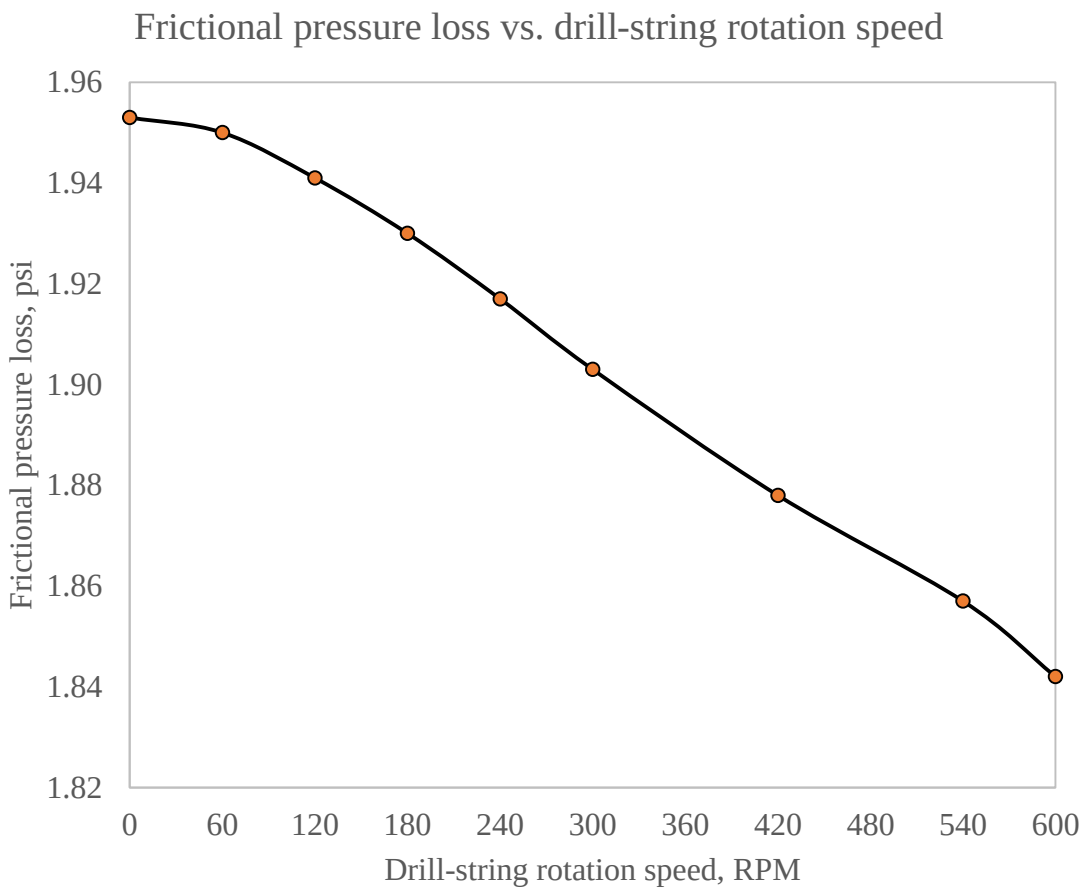

Figure 35: Pressure loss versus drill-string rotation without tool joint

From Table A-4.2 and Figure 35, we can observe that as the drill-string rotation speed increases, the frictional pressure loss decreases steadily from 1.953 psi (0 RPM) to 1.842 psi (600 RPM).

The higher the drill-string rotation speed, the lower the frictional pressure loss.

4.3 Combined Effects of Drill-String Tool Joint and Rotation on Annular Flow Profile and Frictional Pressure Loss

Thirdly, the combined effects of drill-string tool joint and rotation on annular flow profile and frictional pressure loss were investigated. The number of drill-string tool joint ranged from 0 to 2 and the rotation speed ranged from 0 to 600 RPM.

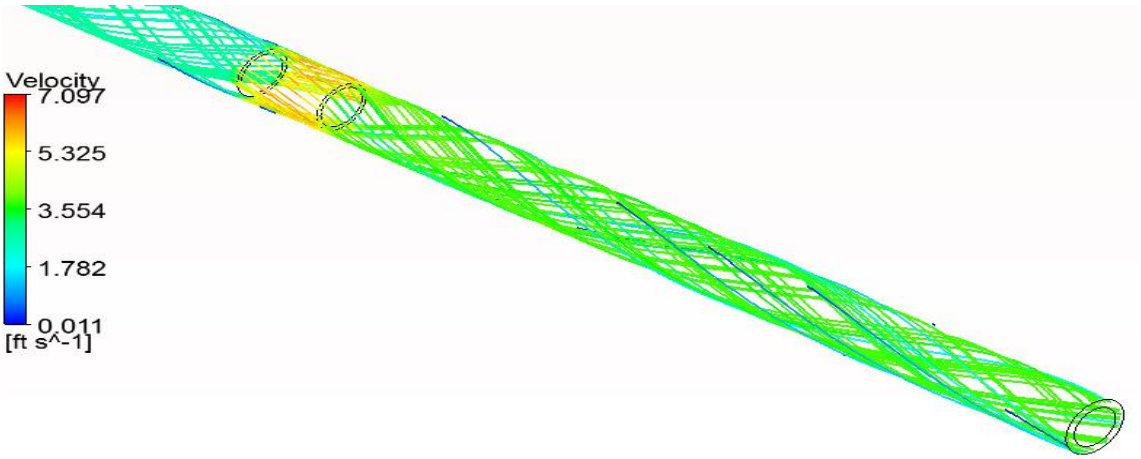

Figure 36: Annular flow profile at 600 RPM with 1 tool joint

Figure 36 presents the collective influence of drill-string tool joint and rotation on the annular flow profile. It is observed that the peak fluid velocity is achieved at the tool joint section, which is 7.097 ft/s. As compared to Figure 28, at 600 RPM and without a tool joint, the fluid velocity is uniform at around 3.941 ft/s. On the other hand, according to Figure 20, at 0 RPM and a tool joint is present, the peak fluid velocity is 6.776 ft/s.

Therefore, the combined effect of drill-sting tool joint and rotation on increasing the fluid velocity is greater than each of the individual factor.

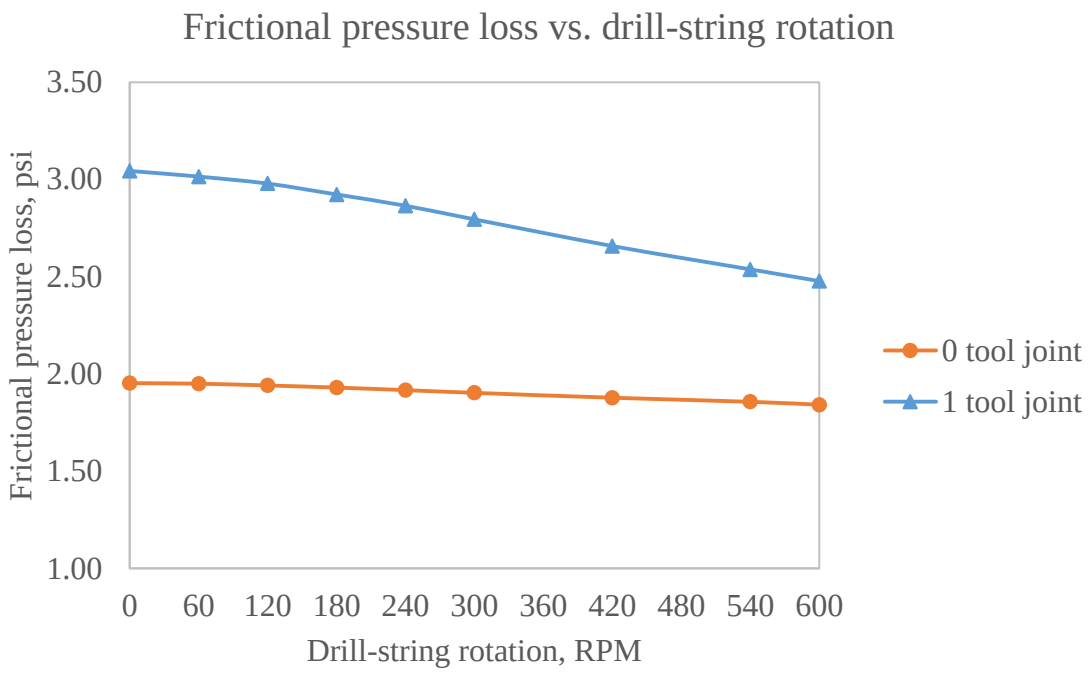

Figure 37: Frictional pressure loss versus drill-string rotation for 0 and 1 tool joint

From Table A-4.3 and Figure 37, we can observe that the frictional pressure loss is always greater when there is a tool joint, as compared to drill-string without tool joint.

We can also observe that the higher the drill-string rotation speed, the lower the frictional pressure loss. Without tool joint, the frictional pressure loss decreases from 1.953 psi to 1.842 psi as the drill-string rotation speed increases from 0 to 600 RPM, which is a 5.7% decrease. With 1 tool joint, the frictional pressure loss decreases from 3.044 psi to 2.478 psi as the drill-string rotation speed increases from 0 to 600 RPM, which is a 18.6% decrease.

The effects of tool joint and drill-string rotation on frictional pressure loss are opposing. The higher the number of tool joint, the higher the frictional pressure loss. The higher the drill-string rotation speed, the lower the frictional pressure loss.

The number of tool joint is the dominant factor which affects the frictional pressure loss, whereas drill-string rotation plays a less significant role.

CHAPTER 5

5. CONCLUSION & RECOMMENDATIONS

5.1 Conclusion

In this project, the hydraulic effects of drill-string tool joint and rotation on annular flow profile and frictional pressure loss are investigated using Computational Fluid Dynamics (CFD) approach, the analysis system is ANSYS-CFX.

The CFD model was created and grid independence study suggested that 0.012 ft is the optimum mesh element size, which minimises simulation time and yet provides similar results as the CFD models with higher number of mesh elements. Benchmarking shows good agreement between the CFD simulation results with experimental results with low mean percentage errors. In addition, the Design of Experiment stage, where case studies based on design points were carried out concluded that

- Annular flow profile is affected by both drill-string tool-joint and rotation.

  The fluid velocity is the highest at the tool joint section, because of the smaller annular space. Dynamic viscosity is the lowest at the tool joint section, because at this section, the fluid velocity is the highest.

  Drill-string rotation causes the fluid to be in a helical motion. The overall fluid velocity is higher under higher drill-string rotation speed. In addition, drill-string rotation greatly increases the velocity of the fluid immediately next to the drill-string outer wall; without rotation, the fluid immediately next to the drill-string outer wall is almost static. The higher the drill-string rotation speed, the lower the overall fluid dynamic viscosity.

- Frictional pressure loss is always greater when a tool joint is present, regardless of the drill-string rotation speed. Frictional pressure loss decreases as the drill-string rotation speed increases, regardless of the presence of tool joint, this observation agrees with the literature [7], [12], [21]. However, the effect of drill-string rotation is more prominent when a tool joint is present. When a tool joint is present, under a particular rotation speed, the frictional pressure loss varies more significantly, as compared to the frictional pressure loss when no tool joint is present.

5.2 Recommendations

In this study, the simulation model assumes isothermal condition, which is not realistic as compared to an actual wellbore with increasing temperature along the depth. Variation in temperature affects the rheology of the drilling mud, which will significantly affect the annular flow profile and frictional pressure loss. Therefore, in the future, a dynamic temperature model may be included into the simulation for more accurate results.

In addition, this study considers only the drilling fluid without the presence of drill cuttings. Drill cuttings will affect the wellbore fluid column density, which will affect the annular flow profile and frictional pressure loss.

Moreover, this study considers horizontal well, deviated well and vertical can be modelled to study the effects of well trajectory on annular flow profile and frictional pressure loss.

Last but not least, open hole has a higher roughness and a more irregular geometry than a cased hole. In this study, the latter is considered. In future, it is recommended to model open hole section to understand how the annular flow profile and frictional pressure loss are affected differently.

REFERENCES

[1] B. Bui, "Modeling the Effect of Pipe Rotation on Pressure Loss through Tool Joint," in *SPETT 2012 Energy Conference and Exhibition*, 2012.

[2] M. Enfis, A. Ramadan. and A. Saasen, "The Hydraulic Effect of Tool-joint on Annular Pressure Loss," in *SPE Production and Operations Symposium*, 2011.

[3] A. P. Singh, and R. Samuel, "Effect of Eccentricity and Rotation on Annular Frictional Pressure Losses With Standoff Devices," in *SPE Annual Technical Conference and Exhibition*, 2009.

[4] A. K. Vajargah, F. N. Fard, M. Parsi and B. B. Hoxha, "Investigating the Impact of the "Tool Joint Effect" on Equivalent Circulating Density in Deep-Water Wells," in *SPE Production and Operations Symposium*, 2014.

[5] Y. T. Jeong and S. N. Shah, "Analysis of Tool Joint Effects for Accurate Friction Pressure Loss Calculations," in *IADC/SPE Drilling Conference*, 2014.

[6] S. G. Bared, "Another Method Depicting the Effect of Rotation of Drillig Fluids in a Pipe on the Pressure Drop," 1990.

[7] S. A. Hansen and N. Sterri, "Drill Pipe Rotation Effects on Frictional Pressure Losses in Slim Annuli," in *SPE Annual Technical Conference & Exhibition*, 1995.

[8] R. C. McCann, M. S. Quigley, M. Zamora and K. S. Slater, "Effects of High-Speed Pipe Rotation on Pressures in Narrow Annuli," *SPE Drilling & Completion*, 1995.

[9] C. D. Marken, X. J. He and A. Saasen, "The Influence of Drilling Conditions on Annular Pressure Losses," in *SPE Annual Technical Conference and Exhibition*, 1992.

[10] D. J. Bode, R. B. Noffke and H. V. Nickens, "The Influence of Drilling Conditions on Annular Pressure Losses," *Journal of Petroleum Technology*, 1991.

[11] R. A. Delwiche, M. W. D. Lejeune, P. F. B. N Mawet and Vighetto, "Slimhole Drilling Hydraulics," in *SPE Annual Technical Conference and Exhibition*, 1992.

[12] R. E. Walker and A. Othmen, "Helical Flow of Bentonite Slurries," in *Fall Meeting of the Society of Petroleum Engineers of AIME*, 1970.

[13] T. Hemphill, P. Bern, J. C. Rojas and K. Ravi, "Field Validation of Drillpipe Rotation Effects on Equivalent Circulating Density," in *SPE Annual Technical Conference and Exhibition*, 2007.

[14] M. E. Ozbayoglu, A. Saasen, M. Sorgun and K. Svanes, "Effect of Pipe Rotation on Hole Cleaning for Water-Based Drilling Fluids in Horizontal and Deviated Wells," in *IADC/SPE Asia Pacific Drilling Technology Conference and Exhibition*, 2008.

[15] A. O. Omosebi and K. A. A. Adenuga, "Pressure Drop versus Flow Rate Profiles for Power-Law and Herschel-Bulkley Fluids," in *Nigeria Annual International Conference and Exhibition*, 2012.

[16] Y. J. Luo and J. M. Peden, "Reduction of Annular Friction Pressure Drop Caused By Drillpipe Rotation," Texas: Society of Petroleum Engineers, 1990.

[17] T. N. Ofei, S. Irawan and W. Pao, "CFD Method for Predicting Annular Pressure Losses and Cuttings Concentration in eccentric Horizontal Wells," in *Journal of Petroleum Engineering*, 2014.

[18] V. Dokhani, M. P. Shahri, M. Karimi and S. Salehi, "Laminar Non-Newtonian Flow in an Eccentric Annulus, a Numerical Solution," in *SPE Annual Technical Conference and Exhibition*, 2013.

[19] S. Simoes, M. Yu, S. Miska and N. E. Takach, "The Effect of Tool Joints on ECD While Drilling," in *SPE Production and Operations Symposium*, 2007.

[20] T. J. Lockett, S. M. Richardson and W. J. Worraker, "The Importance of Rotation Effects for Efficient Cuttings Removal During Drilling," in *SPE/IADC Drilling Conference*, 1993.

[21] S. Chandrasekhar, "Hydrodynamic and Hydromagnetic Stability," Oxford, 1961.

[22] ANSYS, Inc., "ANSYS CFX-Solver Theory Guide," Canonsburg, 2011.

[23] T. N. Ofei, S. Irawan, W. Pao and R. E. Osgouei, "Modified Yield Power-Law Fluid In Narrow Annuli with Inner Rotating Pipe," in *The Canadian Journal Of Chemical Engineering*, 2015.

[24] M. S. Enfis, The Effects of Tool-Joint on Annular Pressure Loss, Oklahoma: University of Oklahoma, 2011.

[25] AMERICAN SOCIETY FOR QUALITY, 'What Is Design of Experiments (DOE)?', 2015. [Online]. Available: http://asq.org/learn-about-quality/data-collection-analysis-tools/overview/design-of-experiments.html. [Accessed: 10- Jan- 2015].

APPENDICES

Appendix 1: ANSYS-CFX Simulation Result Formats

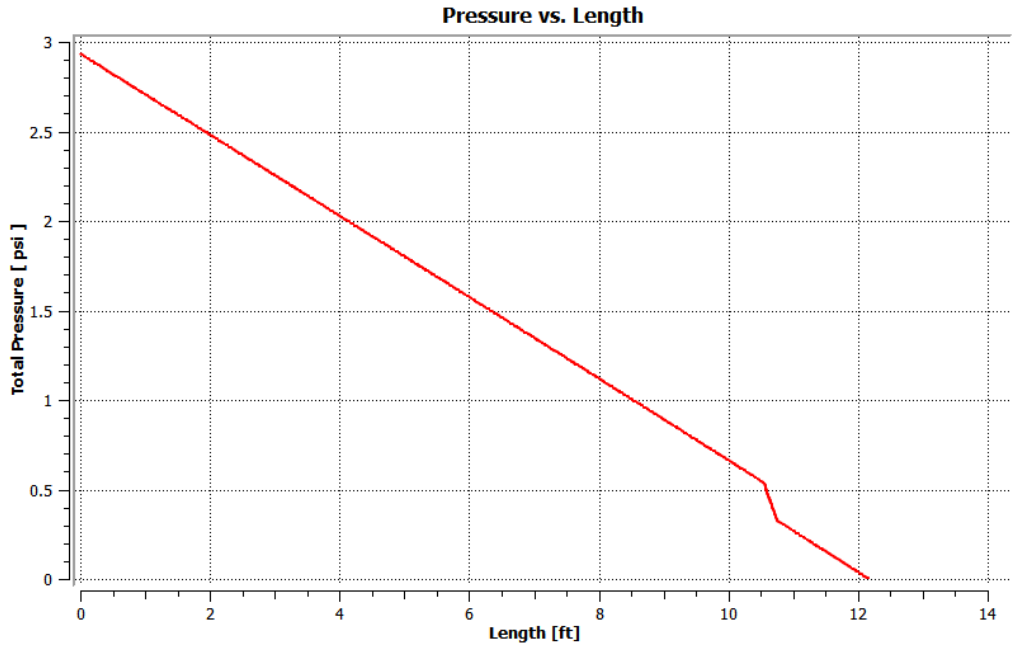

Figure A-1.1: Graph of pressure versus the entire annulus length

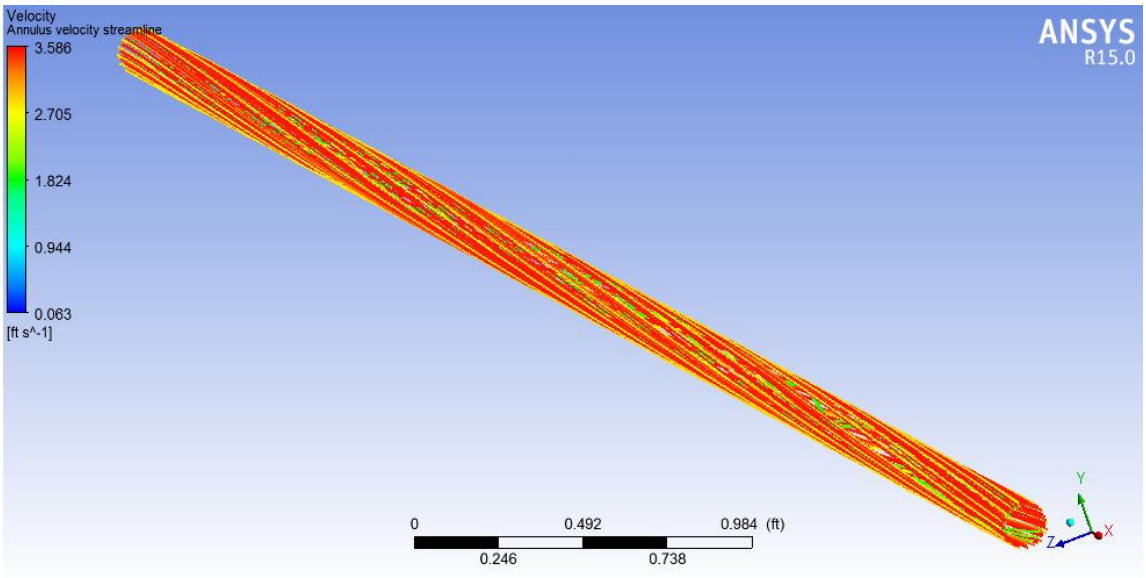

Figure A-1.2: Velocity streamline

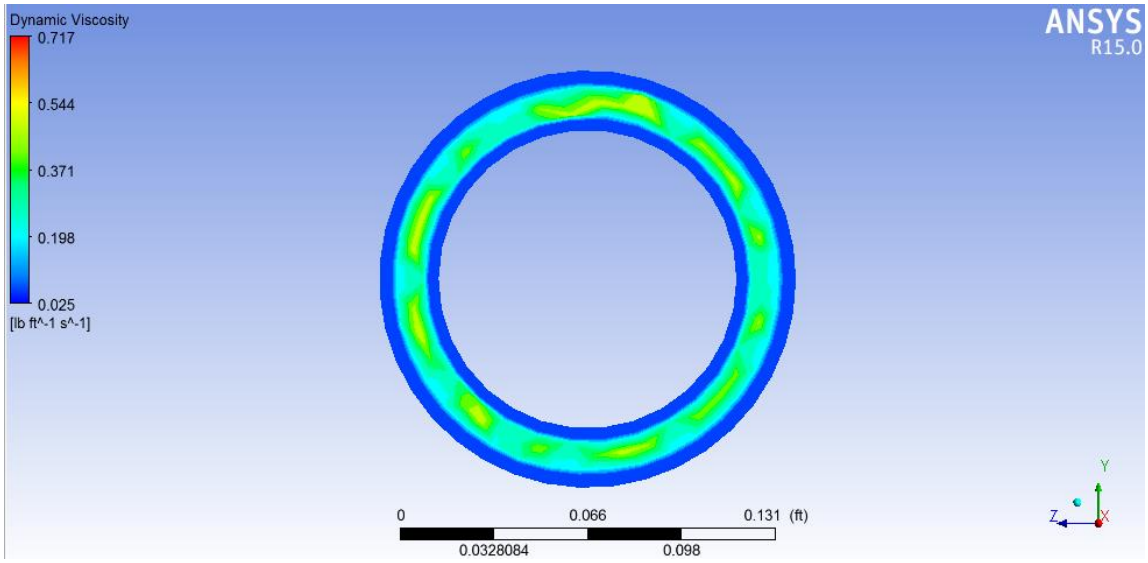

Figure A-1.3: Dynamic viscosity contour

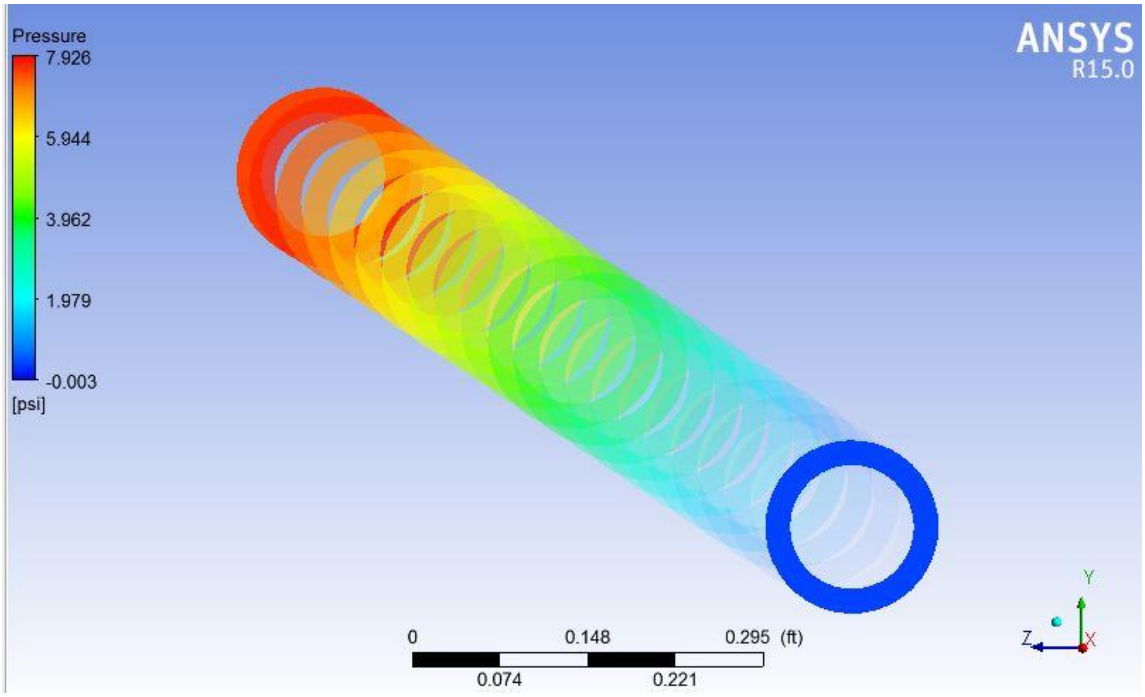

Figure A-1.4: Volume rendering of pressure distribution in CFD-Post

Appendix 2: Benchmarking - CFD Model Adjustments To Improve Benchmarking

Table A-2.1: Adjustments made on CFD model to improve Benchmarking

Adjustments		Effect(s) on CFD simulation result (pressure loss readings)	Improvement on CFD model benchmarking?
Geometry	Add 3 ft of casing and drill-string after outlet.	No effect.	X
	Increase the total length from 12.167 ft to 20 ft by adding the extra length in front of the inlet.	Lower than the experimental data.	X
	Decrease the total length from 12.167 ft to 8.167 ft by cutting the extra length at the inlet.	Lower than the experimental data.	X
Setup: inlet > boundary details > turbulence > option	Use "intensity and auto compute length" option and input different values.	No effect (despite different input values) and does not improve the result to be closer to the experimental data.	X
	Use "high" intensity.	Higher than the experimental data.	X
	Use "zero gradient" intensity.	Lower than the experimental data.	X
Setup: fluid flow rate	Suspected that the thesis may be using UK GPM, upon verification, is US GPM.	-	√
	Compare results when CFD simulation is carried out using flow rate (US GPM) or velocity (ft/s), to ensure Equation 1 is correct.	No effect, use either parameters will yield similar result.	√
Setup: fluid > fluid models > turbulence > k-epsilon > advanced	Increase Ce1 from 1.44 (default) to 2 and 20; Ce2 from 1.92 (default) to 3 & 30.	Lower than the experimental data.	X
	Decrease Ce1 to 0.1 and 0.0001; Ce2 to 0.2 and 0.0001	Lower than the experimental data.	X

turbulence control	Change “curvature correction” from 1 (default) to 30.	No convergence	X
	Change “epsilon flux closure” from 1.3 (default) to 1000	No convergence	X
Setup: fluid > fluid models > Turbulence	K-epsilon	Pressure loss value is more similar to experimental data for higher flow rates.	√
	Laminar	Pressure loss value is more similar to experimental value for lower flow rates.	√
	Shear stress transport / SSG / BSL.	Pressure loss is either too high or too low as compared to experimental data.	X
Setup: outlet > boundary details > mass and momentum	Change pressure profile blend from 0.05 (default) to 0 and 0.5.	Pressure loss is lower than the experimental data. Different blend values have no effect on result.	X
	Change outlet relative pressure from 0 to 1 psi	No effect.	X
Solution: “Reynolds number out of range” warning	During each simulation, if this warning appears, “k-epsilon turbulence model” is used.	-	√

Appendix 3: Benchmarking – Tabulated Results

Table A-3.1: P1: 36” tool joint section pressure loss values at various flow rates for fluid E at 0 RPM (CFD simulation and experimental results)

Operating parameters					
Drill pipe rotation (RPM)	0				
Fluid (refer to Table 4)	E				
P1 (36" tool joint section, 9.167ft – 12.167 ft)					
Flow rate (USGPM)	3.60	6.22	10.75	18.58	26.75
P1 (CFD) (psi)	0.700	0.980	1.430	2.135	2.785
P1 (Experiment) (psi)	0.700	0.990	1.440	2.140	2.770
Percentage Error (%)	0.1	1.0	0.7	0.2	0.5
Mean Percentage Error (%)	0.5				

Table A-3.2: P2: 12” section without tool joint pressure loss values at various flow rates for fluid E at 0 RPM (CFD simulation and experimental results)

P2 (12" section without tool joint, 8 ft – 9 ft)					
Flow rate (USGPM)	3.60	6.22	10.75	18.58	26.75
P1 (CFD) (psi)	0.18	0.26	0.38	0.3	0.412
P1 (Experiment) (psi)	0.16	0.22	0.32	0.46	0.62
Percentage Error (%)	14.0	18.2	18.8	34.8	33.5
Mean Percentage Error (%)	23.9				

Table A-3.3: P3: 12” tool joint section pressure loss values at various flow rates for fluid E at 0 RPM (CFD simulation and experimental results)

P3 (12" tool joint section, 10.167 ft – 11.167 ft)					
Flow rate (USGPM)	3.60	6.22	10.75	18.58	26.75
P1 (CFD) (psi)	0.32	0.45	0.67	1.463	1.912
P1 (Experiment) (psi)	0.35	0.5	0.75	1.21	1.69
Percentage Error (%)	7.5	10.0	10.7	20.9	13.1
Mean Percentage Error (%)	12.4				

Table A-3.4: P2: 12” section without tool joint pressure loss values at various flow rates for fluid G 60 RPM and 180 RPM (CFD simulation and experimental results)

P2 (12" section without tool joint, 8 ft – 9 ft)					
Flow rate (USGPM)	3.55	6.19	10.67	18.52	26.79
Rotation (RPM)	60				
P2 (CFD) (psi)	0.28	0.34	0.48	0.65	0.82
P2 (Experiment) (psi)	0.24	0.29	0.38	0.53	0.69
Percentage Error (%)	2.1	3.4	0	7.5	7.2

Mean Percentage Error (%)	4.1				
Rotation (RPM)	180				
P2 (CFD) (psi)	0.27	0.35	0.49	0.68	0.84
P2 (Experiment) (psi)	0.22	0.29	0.39	0.56	0.75
Percentage Error (%)	0	3.4	2.6	8.9	8.0
Mean Percentage Error (%)	4.6				

Table A-3.5: P3: 12” tool joint section pressure loss values at various flow rates for fluid G for 60 RPM and 180 RPM (CFD simulation and experimental results)

P3 (12" tool joint section, 10.167 ft – 11.167 ft)					
Flow rate (USGPM)	3.55	6.19	10.67	18.52	26.79
Rotation (RPM)	60				
P3 (CFD) (psi)	0.45	0.532	0.752	1.049	1.388
P3 (Experiment) (psi)	0.431095	0.579505	0.848057	1.30742	1.84452
Percentage Error (%)	0	1.7	9.4	7.6	8.2
Mean Percentage Error (%)	5.4				
Rotation (RPM)	180				
P3 (CFD) (psi)	0.43	0.559	0.773	1.102	1.433
P3 (Experiment) (psi)	0.4311	0.5795	0.8481	1.3145	1.7739
Percentage Error (%)	0	3.4	16.5	10.7	14.7
Mean Percentage Error (%)	9.1				

Appendix 4: Design of Experiment – Tabulated Results

Table A-4.1: Frictional pressure loss due to tool joint(s) at 0 RPM drill-string rotation speed

Factor	Response	Remark
Number of tool joint	Frictional pressure loss (8.667 – 11.667 ft) (psi)	
0	1.953	Drill-string rotation speed is 0 RPM.
1	3.044	
2	3.976	

Table A-4.2: Frictional pressure loss due to drill-string rotation without tool joint

Factor	Response	Remark
Drill-string rotation speed (RPM)	Pressure loss (8.667 – 11.667 ft) (psi)	
0	1.953	Drill-string has no tool joint.
60	1.950	
120	1.941	
180	1.930	
240	1.917	
300	1.903	
420	1.878	
540	1.857	
600	1.842	

Table A-4.3: Frictional pressure loss due to drill-string tool joint(s) and rotation

Factors		Response
Number of tool joint	Drill-string rotation speed (RPM)	Pressure loss (8.667 – 11.667 ft) (psi)
0	0	1.953
	60	1.950
	120	1.941
	180	1.930
	240	1.917
	300	1.903
	420	1.878
	540	1.857
	600	1.842
1	0	3.044
	60	3.015
	120	2.979
	180	2.923
	240	2.865
	300	2.795
	420	2.658
	540	2.538
	600	2.478